SIAM J. SCI. COMPUT.
Vol. 31, No. 2, pp. 987–1015

MULTIBODY INTERACTIONS IN COARSE-GRAINING SCHEMES FOR EXTENDED SYSTEMS*

SASANKA ARE†, MARKOS A. KATSOULAKIS†, PETR PLECHÁČ‡, AND LUC REY-BELLET†

Abstract. In this paper we address the role of multibody interactions for the coarse-grained approximation of stochastic lattice systems. Such interaction potentials are often not included in coarse-graining schemes, as they can be computationally expensive. The multibody interactions are obtained from the error expansion of the reference measure which is, in many cases, chosen as a Gibbs measure corresponding to a local mean-field approximation. We identify the parameter ϵ that characterizes the level of approximation and its relation to the underlying interaction potential. The error analysis suggests strategies to overcome the computational costs due to evaluations of multibody interactions by additional approximation steps with controlled errors. We present numerical examples demonstrating that the inclusion of multibody interactions shows substantial improvement in dynamical simulations, e.g., of rare events and metastability in phase transitions regimes.

Key words. coarse-graining, relative entropy, lattice spin systems, Monte Carlo method, Gibbs measure, cluster expansion, multibody interactions, renormalization group map

AMS subject classifications. 65C05, 65C20, 82B20, 82B80, 82-08

DOI. 10.1137/080713276

1. Introduction.

Molecular dynamics (MD) or Monte Carlo (MC) methods have been used to simulate microscopic systems with complex interactions in a broad spectrum of scientific disciplines. However, one of the main hurdles in the computations with such methods are the difficulties that arise in simulating such molecular systems for spatio-temporal scales of realistic size. In this paper we analyze a particular class of methods known as coarse-graining, a methodology that has been developed in statistical physics for systematic reduction of degrees of freedom.

Coarse-grained models, when compared to original microscopic systems, have fewer observables while at the same time are expected to accurately describe the unresolved degrees of freedom through a proper inclusion of stochastic fluctuations. For example, in polymer science a sophisticated array of methods has been developed systematically grouping several atoms on a macromolecule creating a new, effective chain [2, 4, 6, 23]. Such coarse-graining strategies are designed to describe the complex microscopic short- and long-range interactions at the coarse level while making a few ad hoc assumptions. For example, in the coarse-grained united atom models [4], the coarse interactions between two macromolecules are assumed to be independent of the

*Received by the editors January 14, 2008; accepted for publication (in revised form) July 28, 2008; published electronically November 26, 2008.
http://www.siam.org/journals/sisc/31-2/71327.html

†Department of Mathematics & Statistics, University of Massachusetts, Amherst, MA 01003-1305 (are@math.umass.edu, markos@math.umass.edu, luc@math.umass.edu). The research of the first and second authors was partially supported by the National Science Foundation under grants NSF-DMS-0413864 and NSF-DMS-0715125 and the U.S. Department of Energy under grant DE-FG02-05ER25702. The research of the fourth author was partially supported by the National Science Foundation under grant NSF-DMS-0605058.

‡Department of Mathematics, University of Tennessee, Knoxville, TN 37996-1300 (plechac@math.utk.edu). The research of this author was partially supported by the National Science Foundation under grant NSF-DMS-0303565 and by the Office of Advanced Scientific Computing Research, U.S. Department of Energy; the work was partly done at the ORNL, which is managed by UT-Battelle, LLC under contract DE-AC05-00OR22725.

rest of the molecules/atoms in the polymer chain. In essence this procedure eliminates multibody interactions of the coarse-grained potential. One of the main focus points of this paper is to address the role of the multibody interactions in coarse-graining. In particular, in section 6, we specifically discuss the relation between the coarse-graining of the united atom model and the coarse-graining schemes presented here.

The approach studied in this paper is based on the coarse-graining schemes for stochastic lattice systems such as an Ising-type model that were developed in [14]. This class of stochastic lattice processes is employed in the modeling of adsorption, desorption, reaction, and diffusion of chemical species in application areas such as catalysis, microporous materials, biological systems, etc. [18, 3].

The microscopic system consists of a lattice Λ_N with N sites. At each site $x \in \Lambda_N$ we define an order parameter $\sigma(x)$. For instance, when it takes values 0 and 1, it can describe vacant and occupied sites. The energy $H_N(\sigma)$ of the system, at the configuration $\sigma = \{\sigma(x) : x \in \Lambda_N\}$, is given by the Hamiltonian

$$H_N(\sigma) = -\frac{1}{2}\sum_{x\in\Lambda_N}\sum_{y\neq x} J(x-y)\sigma(x)\sigma(y) + \sum_{x\in\Lambda_N} h(x)\sigma(x)\,, \tag{1.1}$$

where h denotes the external field and J defines the interparticle potential. Equilibrium states at the temperature T are described by the (canonical) Gibbs measure

$$\mu_{N,\beta}(d\sigma) = \frac{1}{Z_N} e^{-\beta H_N(\sigma)} P_N(d\sigma)\,, \tag{1.2}$$

where $\beta = 1/kT$ (with the Boltzmann constant k), Z_N is the partition function, and $P_N(d\sigma)$ is the prior Bernoulli measure. In this setting the coarse-graining can be carried out by subdividing the lattice into coarse cells and defining coarse-grained variables using a corresponding map $\mathbf{F}$,

$$\eta(k) := \mathbf{F}(\sigma)(k) = \sum_{x\in C_k} \sigma(x)\,, \tag{1.3}$$

on each coarse cell C_k; see section 2.2 and Figure 1. The corresponding renormalization group map, known as the Kadanoff transform [5, 7], is defined by the formula

$$e^{-\beta \bar{H}_M(\eta)} = \int e^{-\beta H_N(\sigma)} P_N(d\sigma|\eta)\,, \tag{1.4}$$

where $\bar{H}_M(\eta)$ represents the exactly coarse-grained Hamiltonian and $P_N(d\sigma|\eta)$ is the conditional probability of having a microscopic configuration σ given a configuration η at the coarse level. However, due to the high-dimensional integration, $\bar{H}_M(\eta)$ cannot be easily calculated explicitly and hence used in numerical simulations. The main idea in [14] is to write the exact coarse-grained Hamiltonian $\bar{H}_M(\eta)$ as a perturbation around the first approximation Hamiltonian $\bar{H}_M^{(0)}$. The first approximation $\bar{H}_M^{(0)}$, suggested in [9, 10], is defined as

$$\bar{H}_M^{(0)}(\eta) = \int H_N(\sigma) P_N(d\sigma|\eta)\,. \tag{1.5}$$

Alternative approximations arising in the polymer science literature are discussed in section 6. Using the approximation (1.5) we have from (1.4) that

$$\bar{H}_M(\eta) \;=\; \bar{H}_M^{(0)}(\eta) - \frac{1}{\beta}\log \int e^{-\beta(H_N(\sigma) - \bar{H}_M^{(0)}(\eta))} P_N(d\sigma|\eta)\,. \tag{1.6}$$

The error analysis was studied in [14], where the authors showed that under suitable assumptions $\bar{H}_M(\eta)$ can be written as a convergent series expansion around $\bar{H}_M^{(0)}(\eta)$. Since $\bar{H}_M(\eta)$ scales as $\mathcal{O}(N)$, the expression (1.6) cannot be expanded by using a simple Taylor expansion, but instead a cluster expansion (see, e.g., [22]) is necessary to obtain the following series:

$$\bar{H}_M(\eta) - \bar{H}_M^{(0)}(\eta) = \bar{H}_M^{(1)}(\eta) + \cdots + \bar{H}_M^{(\alpha)}(\eta) + N\mathcal{O}(\epsilon^{\alpha+1}), \quad \alpha = 2, \dots, \tag{1.7}$$

which converges uniformly in η. Furthermore, the correction terms $\bar{H}_M^{(1)}(\eta)$, $\bar{H}_M^{(2)}(\eta)$, etc., are calculated explicitly. The parameter ϵ depends on the characteristics of the coarse-graining, the potential, and the inverse temperature. We also note that since the Hamiltonian is an extensive quantity (of order N), the error term in (1.7) is also expected to scale with N. We shall see in section 2.4 that three-body interactions are included in the $\bar{H}_M^{(2)}(\eta)$ term.

The next step in developing a successful approximation strategy requires understanding the error from coarse-graining. For example, (over-)coarse-graining in polymer systems may yield wrong predictions in the melt structure [1]; similarly, wrong predictions on crystallization were observed in the coarse-graining of complex fluids [21]. The error arising in any attempt to coarse-grain microscopic systems essentially involves the comparison of the coarse-grained probability measures to the projection of the microscopic measure on the coarse variables. One way to quantify the error from coarse-graining is to estimate the relative entropy between these measures. In information theory the relative entropy $\mathcal{R}(\pi_1 \,|\, \pi_2)$ provides a measure of "information loss" in the approximation of the probability measure π_1 by π_2; see, e.g., [16, 14]. The relative entropy of π_1 with respect to π_2, for $\pi_1(\sigma)$ and $\pi_2(\sigma)$ two probability measures defined on a common countable state space $\mathcal{S}$, is defined as

$$\mathcal{R}(\pi_1 \,|\, \pi_2) = \sum_{\sigma \in \mathcal{S}} \pi_1(\sigma) \log \frac{\pi_1(\sigma)}{\pi_2(\sigma)}.$$

In our context, we use the relative entropy in order to assess the information compression of different coarse-graining schemes; see Scheme 2.1 in section 2.4. Furthermore, since we are dealing with extensive systems and compressing local interactions, the errors are also extensive quantities, and it is thus natural to measure the error per unit volume, i.e., in terms of the relative entropy per unit volume. For example, the relative entropy of the Gibbs measure $\bar{\mu}_{M,\beta}^{(\alpha)}$ associated with the Hamiltonian $\bar{H}_M^{(\alpha)}(\eta)$, with respect to the Gibbs measure $\mu_{N,\beta} \circ \mathbf{F}^{-1}$ associated with the Hamiltonian $\bar{H}_M(\eta)$ (see Scheme 2.2), is given by

$$\frac{1}{N}\mathcal{R}(\bar{\mu}_{M,\beta}^{(\alpha)} | \mu_{N,\beta} \circ \mathbf{F}^{-1}) \sim \mathcal{O}(\epsilon^{\alpha+1}).$$

In this work we first identify the parameter ϵ corresponding to the coarse-graining, the type of interaction potential, and the inverse temperature, β. The particle interactions discussed are power laws, Coulomb, logarithmic, and combined short- and long-range potentials which are of relevance in various lattice models. The estimates derived on the coarse-grained methods allow us to compare the relative size and importance of two-body coarse-grained interactions included in $\bar{H}_M^{(0)}$, $\bar{H}_M^{(1)}$ to three-body coarse-grained interactions given by $\bar{H}_M^{(2)}$.

However, implementing a higher-order coarse-graining scheme, which includes multibody interactions, in the case of long-range potentials can be computationally

expensive. Error estimates presented for Scheme 2.1 along with the dependence on the small parameter ϵ discussed in section 3 suggest that we can address the issue of the computational complexity of three-body coarse-grained interactions in two ways: (a) truncate and compress the three-body terms within a given tolerance (section 3.4.1), or (b) split the interaction potential J in (1.1) into a short-range piece with possible singularities and a smooth long-range component. The analysis in section 3 shows that if the potential is smooth, long-range, and with appropriate decay, then the error from the two-body coarse-graining using the Hamiltonian $\bar{H}_M^{(0)}$ is small. On the other hand, the three-body corrections are necessary in the case of the short-range potential with possible singularities. In such a case the 3rd-order accurate method of Scheme 2.2 is to be applied.

In an earlier paper [14] we primarily dealt with coarse-graining of stochastic lattice systems at equilibrium. A distinct focus of the numerical simulations in this paper is on the role of the multibody coarse-grained interactions in approximating the coarse-grained dynamics. It was observed in [9] that for long-range interactions the 2nd-order coarse-graining scheme was able to accurately capture dynamics related behavior of coarse observables at certain parameter regimes. However, when studying dynamical properties, e.g., mean times to phase transition, the error from coarse-graining increased substantially especially as the level of coarse-graining increased [11]. The numerical experiments in section 5 show that the inclusion of multibody interactions is critical for accurately reproducing dynamical properties involving rare events such as switching times.

The paper is organized as follows. In section 2 we present the microscopic model and motivate different coarse-graining schemes. In section 3 we focus on error quantification by identifying the parameter ϵ in the coarse-grained approximation. We also discuss the relative size and importance of the multibody interactions using estimates derived for specific potentials. In section 4 we give a description of the kinetic MC dynamics and algorithms used for generating the microscopic and the coarse-grained processes. In section 5 we present simulations with different coarse-graining schemes using the Arrhenius spin-flip dynamics. Finally, in section 6, we present a discussion on the relation of analyzed schemes to coarse-graining schemes used for macromolecular systems.

2. Equilibrium. In this section we present the coarse-graining at equilibrium for an Ising-type system. We discuss the microscopic model defined by the Hamiltonian $H_N(\sigma)$ (1.1) and the corresponding Gibbs measure $\mu_{N,\beta}$ (1.2), followed by the coarse-graining procedure and the exact coarse-grained Hamiltonian, $\bar{H}_M(\eta)$. Using formal calculations we motivate the derivation of the first approximation $\bar{H}_M^{(0)}(\eta)$ and a cluster expansion of $\bar{H}_M(\eta)$ (1.7) around the first approximation $\bar{H}_M^{(0)}(\eta)$. Finally, we present the numerical schemes for coarse-graining with the corresponding error estimates.

2.1. Microscopic models. The domain of the microscopic system Λ_N includes N sites and is a subset of the rescaled square lattice $(\frac{1}{n}\mathbb{Z})^d$ with lattice constant $1/n$. In order to simplify our presentation we will mainly consider the example $\Lambda_N := (\frac{1}{n}\mathbb{Z})^d \cap \mathbb{T}_d$, where $\mathbb{T}_d := [0,1)^d$ is the d-dimensional torus, and the number of lattice sites $N = n^d$ is fixed but arbitrary and finite. Although here we consider a periodic domain, other boundary conditions can be accommodated easily. The spin (or order parameter) $\sigma(x)$ takes values in $\{0,1\}$ at each lattice site $x \in \Lambda_N$. A spin configuration $\sigma = \{\sigma(x)\}_{x\in\Lambda_N}$ is an element of the configuration space $\mathcal{S}_N := \{0,1\}^{\Lambda_N}$. The energy

of the configuration σ is given by the Hamiltonian $H_N(\sigma)$, defined in (1.1).

The strength of the potential is measured by $\| J \| \equiv \sum_{x \neq 0} |J(x)|$; i.e., we assume that the two-body potential is summable in the thermodynamic limit $N \to \infty$. In section 3 we discuss several examples of potentials categorized in a way relevant for the numerical treatment of coarse-graining approximations.

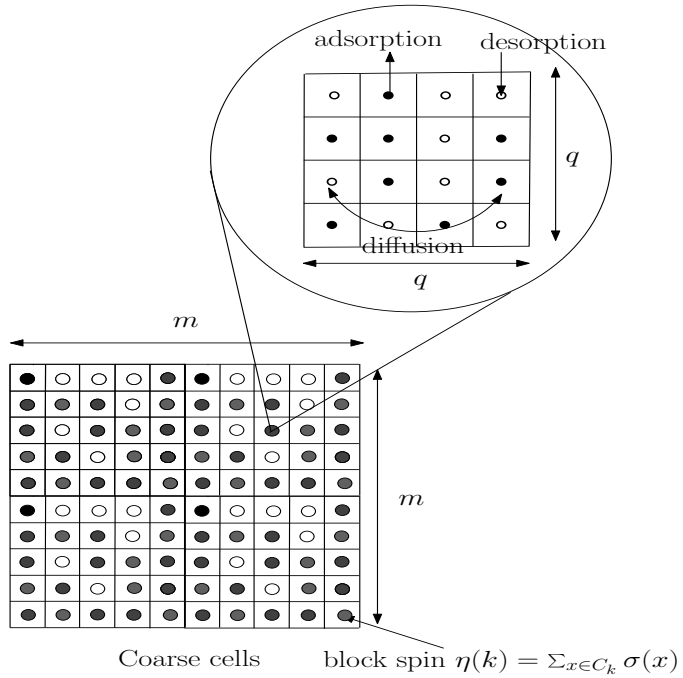

FIG. 1. *Schematic of microscopic and coarse-grained lattices and dynamics in two dimensions.*

2.2. Coarse-grained models. The coarse-graining procedure consists of three main steps:

(a) *Coarse graining of the configuration space.* We partition the torus $\mathbb{T}_d$ into $M = m^d$ cells: For $k = (k_1, \ldots, k_d) \in \mathbb{Z}^d$ with $0 \leq k_i \leq m-1$, we define $C_k \equiv [\frac{k_1}{m}, \frac{k_1+1}{m}) \times \cdots \times [\frac{k_d}{m}, \frac{k_d+1}{m})$ and we have $\mathbb{T}_d = \cup_k C_k$. We identify each cell C_k with a lattice point of the coarse lattice $\bar{\Lambda}_M = (\frac{1}{m}\mathbb{Z})^d \cap \mathbb{T}_d$. Each coarse cell contains $Q = q^d$ points of the microscopic lattice points with $N \equiv n^d = (mq)^d \equiv MQ$. We will refer to Q as the level of coarse-graining ($Q = 1$ corresponds to no coarse-graining). We define a distance function between the coarse cells C_k and C_l:

$$r_{|k-l|} = \frac{1}{m} \left(\sum_{i=1}^{d} (k_i - l_i)^2 \right)^{\frac{1}{2}}, \quad k, l \in \mathbb{Z}^d \text{ with } 0 \leq k_i, l_i \leq m-1 \,.$$

We assign a new spin value $\eta(k)$ for the cell C_k according to the rule

$$\eta(k) := \mathbf{F}(\sigma)(k) = \sum_{x \in C_k} \sigma(x) \,.$$

The spin $\eta(k)$ takes values in $\{0, 1, 2, \ldots, Q\}$, and the configuration space for the coarse-grained system is $\bar{\mathcal{S}}_M \equiv \{0, 1, 2, \ldots, Q\}^{\bar{\Lambda}_M}$. The coarse and the fine lattices are depicted in Figure 1.

(b) *Coarse-graining of the prior distribution.* The prior distribution P_N on $\mathcal{S}_N$ induces a new prior distribution on $\bar{\mathcal{S}}_M$ given by $\bar{P}_M(\eta) = P_N(\sigma : \mathbf{F}(\sigma) = \eta)$. The conditional probability $P_N(d\sigma|\eta)$, defined in (1.4), plays a crucial role in the definition of a coarse-grained Hamiltonian. Since $\eta(k)$ depends only on the spins $\sigma(x)$, $x \in C_k$, the probability $P_N(d\sigma|\eta)$ factorizes over the coarse cells. We have the following expectations, assuming in each case that all spin sites $x, y, x', y' \in C_k$ are different and that $\eta(k) = \eta$:

$$E_1(\eta) := \mathbb{E}[\sigma(x)|\eta] = \frac{\eta}{Q}, \tag{2.1}$$

$$E_2(\eta) := \mathbb{E}[\sigma(x)\sigma(x')|\eta] = \frac{\eta(\eta-1)}{Q(Q-1)}, \tag{2.2}$$

$$E_3(\eta) := \mathbb{E}[\sigma(x)\sigma(x')\sigma(y)|\eta] = \frac{\eta(\eta-1)(\eta-2)}{Q(Q-1)(Q-2)}, \tag{2.3}$$

$$E_4(\eta) := \mathbb{E}[\sigma(x)\sigma(x')\sigma(y)\sigma(y')|\eta] = \frac{\eta(\eta-1)(\eta-2)(\eta-3)}{Q(Q-1)(Q-2)(Q-3)}. \tag{2.4}$$

These expectations are used in defining the coarse-graining schemes, which we present in section 2.4.

(c) *Coarse-graining of the Hamiltonian.* We want to construct a new Hamiltonian $\bar{H}_M(\eta)$ at the coarse level. A natural definition of such a Hamiltonian at a coarse level, which we refer to as the *exact* coarse-grained Hamiltonian $\bar{H}_M(\eta)$, is given by (1.4). Even for moderately large values of N the exact computation of $\bar{H}_M(\eta)$ using (1.4) is, in general, impractical. Therefore we want to have a systematic way of calculating explicit approximations of the coarse-grained Hamiltonian $\bar{H}_M$ to any given degree of accuracy. The main idea is to express $\bar{H}_M$ as a perturbation of an approximation $\bar{H}_M^{(0)}(\eta)$; i.e., we write the *exact* coarse-graining $\bar{H}_M$ as

$$\bar{H}_M - \bar{H}_M^{(0)}(\eta) = \bar{H}_M^{(1)}(\eta) + \cdots + \bar{H}_M^{(p)}(\eta) + N\mathcal{O}(\epsilon^{p+1}), \tag{2.5}$$

where ϵ is a parameter depending on the characteristics of the coarse-graining that will be precisely identified in section 3. In the next subsection, we formally answer the following questions:

1. How and why do we choose the first approximation $\bar{H}_M^{(0)}(\eta)$?
2. Once we have $\bar{H}_M^{(0)}(\eta)$, how good is it and how do we measure the error?
3. Can we derive higher-order coarse-graining schemes by calculating the higher-order terms in (2.5)?

2.3. Formal calculations. Suppose we have already chosen $\bar{H}_M^{(0)}(\eta)$; then we can rewrite the exact coarse-graining as a perturbation of $\bar{H}_M^{(0)}(\eta)$ as

$$e^{-\beta \bar{H}_M(\eta)} = e^{-\beta \bar{H}_M^{(0)}(\eta)} \mathbb{E}[e^{-\beta(H_N(\sigma) - \bar{H}_M^{(0)}(\eta))}|\eta]$$

or, equivalently, in terms of the Hamiltonian

$$\bar{H}_M(\eta) - \bar{H}_M^{(0)}(\eta) = -\frac{1}{\beta} \log \mathbb{E}[e^{-\beta(H_N(\sigma) - \bar{H}_M^{(0)}(\eta))}|\eta]\,. \tag{2.6}$$

Now if we formally expand the exponential in the second term in (2.6), then we obtain

$$\mathbb{E}[e^{-\beta(H_N(\sigma) - \bar{H}_M^{(0)}(\eta))}|\eta] = 1 + \mathbb{E}[-\beta\Delta H|\eta] + \frac{1}{2}\mathbb{E}[(-\beta\Delta H)^2|\eta] + \cdots, \tag{2.7}$$

where $\Delta H = H_N(\sigma) - \bar{H}_M^{(0)}(\eta)$. We have from (2.7) that a natural choice for $\bar{H}_M^{(0)}(\eta)$ that is expected to minimize the error should be such that

$$\mathbb{E}[\Delta H|\eta] = 0\,. \tag{2.8}$$

Hence the first approximation $\bar{H}_M^{(0)}$ of the coarse-grained Hamiltonian $\bar{H}_M$ is given by the formula

$$\bar{H}_M^{(0)}(\eta) \equiv \mathbb{E}[H_N|\eta]\,. \tag{2.9}$$

Thus, using (2.1) and (2.2), we have

$$\bar{H}_M^{(0)}(\eta) = -\frac{1}{2}\sum_k \sum_{l\neq k} \bar{J}(k,l)\eta(k)\eta(l) - \frac{1}{2}\sum_k \bar{J}(0)\eta(k)(\eta(k)-1) + h\sum_k \eta(k),$$

where

$$\bar{J}(k,l) := \frac{1}{Q^2}\sum_{x\in C_k, y\in C_l} J(x-y) \quad \text{for } k\neq l,$$
$$\bar{J}(k,k) := \bar{J}(0) = \frac{1}{Q(Q-1)}\sum_{x,y\in C_k, y\neq x} J(x-y) \quad \text{for } k = l.$$

Now that we have defined $\bar{H}_M^{(0)}(\eta)$, we proceed to express the *exact* coarse-grained Hamiltonian $\bar{H}_M(\eta)$ as a perturbation of this first approximation. If $\mathbf{F}(\sigma) = \eta$, then we can write the difference $H_N(\sigma) - \bar{H}_M^{(0)}(\eta)$ as

$$H_N(\sigma) - \bar{H}_M^{(0)}(\eta) = \sum_k \sum_{l\neq k} \Delta_{kl} J(\sigma)\,, \quad \text{where}$$
$$\Delta_{kl} J(\sigma) := -\frac{1}{2}\sum_{\substack{x\in C_k \\ y\in C_l, y\neq x}} (J(x-y) - \bar{J}(k,l))\sigma(x)\sigma(y)\,. \tag{2.10}$$

The expectation in the second term in (2.7) becomes

$$\mathbb{E}[e^{-\beta(H_N(\sigma)-\bar{H}_M^{(0)}(\eta))}|\eta] = \mathbb{E}[\,e^{\sum_{k,l} -\beta\Delta_{kl}J(\sigma)}|\eta] = \mathbb{E}\left[\prod_{k,l} e^{-\beta\Delta_{kl}J(\sigma)}|\eta\right]. \tag{2.11}$$

Formally, the Taylor expansion of the logarithm enables us to write the right-hand term of (2.6) as

$$\begin{aligned}\frac{1}{\beta}\log\mathbb{E}[e^{-\beta(H_N(\sigma)-\bar{H}_M^{(0)}(\eta))}|\eta] &= \frac{1}{\beta}\log\int \prod_{k,l} e^{-\beta\Delta_{kl}J(\sigma)} P_N(d\sigma|\eta) \\ &= \frac{1}{\beta}\log\int\prod_{k,l}\left(1+\sum_{p=1}^{\infty}\frac{1}{p!}(-\beta\Delta_{kl}J(\sigma))^p\right)\prod_k \tilde{\rho}_k(d\sigma) \\ &=: \bar{H}_M^{(1)}(\eta) + \bar{H}_M^{(2)}(\eta) + \cdots\,. \end{aligned} \tag{2.12}$$

Note that the difference $\Delta H = H_N(\sigma) - \bar{H}_M^{(0)}(\eta)$ is an extensive quantity, and hence it is not necessarily small. It is in fact of order $N\epsilon$; hence all of the preceding expansions

should be understood as formal. A rigorous treatment relies on the method of cluster expansions that has been developed in the statistical mechanics literature [22]. Cluster expansions represent a tool which allows for expanding such quantities rigorously in convergent power series using the independence properties of product measures. The crucial fact here is that the conditional measure $P_N(d\sigma|\eta)$ factorizes over the coarse cells. In the next section we present the coarse-graining schemes derived using cluster expansions. We refer the reader to [14] for a detailed theoretical description and analysis of this procedure.

2.4. Coarse-graining schemes. Before we proceed to the statement of numerical schemes we first introduce some notation as suggested by the calculations in section 2.3. To calculate the higher-order corrections requires the expansion of the terms in (2.12) which involve the following quantities:

$$j^1_{kl} := \sum_{\substack{x\in C_k\\ y\in C_l}} (J(x-y)-\bar{J}(k,l))^2, \tag{2.13}$$

$$j^2_{kl} := \sum_{\substack{x\in C_k\\ y,y'\in C_l}} (J(x-y)-\bar{J}(k,l))(J(x-y')-\bar{J}(k,l)), \tag{2.14}$$

$$j^2_{k_1k_2k_3} := \sum_{\substack{x\in C_{k_1}\\ y\in C_{k_2},z\in C_{k_3}}} (J(x-y)-\bar{J}(k_1,k_2))(J(y-z)-\bar{J}(k_2,k_3))\,. \tag{2.15}$$

If $k_1 = k_2$, then we also impose that for $x, y \in C_{k_1}$ we have $y \neq x$. Note also that these quantities have various symmetries: for example, $j^2_{lk} = j^2_{kl}$ or $j^1_{kl} = \tilde{j}^1_{k-l} = \tilde{j}^1_{l-k}$ for some function $\tilde{j}^1$, and similarly j^2_{kl} depends only on $|k-l|$; moreover, $j^2_{k_1k_2k_3} = \tilde{j}^2_{k_1-k_2,k_3-k_2}$.

As suggested by (2.6) and (2.11), we can define as ϵ a parameter that is proportional to $|H_N(\sigma) - \bar{H}^{(0)}_M(\eta)|$ and also dependent on the inverse temperature β:

$$\epsilon \equiv \frac{\beta}{N}\max_{\sigma}|H_N(\sigma) - \bar{H}^{(0)}_M(\eta)|\,. \tag{2.16}$$

Next, we present 2nd- and 3rd-order schemes in terms of their respective accuracy in relative entropy.

SCHEME 2.1 (2nd-order, two-body CG interactions). *The 2nd-order coarse-graining algorithm has the following characteristics:*

1. *The Hamiltonian $\bar{H}^{(0)}_M$, given by* (2.9)*, is written as*

$$\bar{H}^{(0)}_M(\eta) = \sum_{k\neq l}\Lambda^{(0)}_2(k,l;\,\eta(k),\eta(l)) + \sum_k \Lambda^{(0)}_1(k;\,\eta(k)),$$

where

$$\Lambda^{(0)}_2(k,l;\,\eta(k),\eta(l)) = -\frac{1}{2}\bar{J}(k,l)\eta(k)\eta(l),$$
$$\Lambda^{(0)}_1(k;\,\eta(k)) = -\frac{1}{2}\bar{J}(0,0)\eta(k)(\eta(k)-1) + h\eta(k).$$

2. *The Gibbs measure $\bar{\mu}^{(0)}_{M,\beta}$ is given by $\bar{\mu}^{(0)}_{M,\beta}(d\eta) = \frac{1}{\bar{Z}^{(0)}_M} e^{-\bar{H}^{(0)}_M}\bar{P}_M(d\eta)$.*
3. *The relative entropy error is*

$$\frac{1}{N}\mathcal{R}(\bar{\mu}^{(0)}_{M,\beta}|\mu_{N,\beta}\circ\mathbf{F}^{-1}) \sim \mathcal{O}(\epsilon^2)\,.$$

SCHEME 2.2 (3rd-order, multibody CG interactions). *The 3rd-order coarse-graining algorithm has the following characteristics:*

1. *The Hamiltonian* $\bar{H}_M^{(0)} + \bar{H}_M^{(1)} + \bar{H}_M^{(2)}$ *with the correction terms is*

$$\bar{H}_M^{(1)}(\eta) = \sum_{k<l} \Lambda_2^{(1)}(k,l;\,\eta(k),\eta(l)) + \sum_k \Lambda_1^{(1)}(k;\,\eta(k))\,,$$

where

$$\begin{aligned}\Lambda_2^{(1)}(k,l;\,\eta(k),\eta(l)) = \frac{\beta}{2}\big(&j_{kl}^1\,[E_2(\eta(k))E_2(\eta(l)) - E_1(\eta(k))E_2(\eta(l))\\ &- E_2(\eta(k))E_2(\eta(l)) + E_1(\eta(k))E_1(\eta(l))]\\ &+ j_{kl}^2\,[-2E_2(\eta(k))E_2(\eta(l)) + E_2(\eta(k))E_1(\eta(l))\\ &+ E_1(\eta(k))E_2(\eta(l))]\,\big)\,,\\ \Lambda_1^{(1)}(k;\,\eta(k)) = \frac{\beta}{8}\big(&4j_{kk}^2\,[-E_4(\eta(k)) + E_3(\eta(k)]\\ &+ 2j_{kk}^1\,[E_4(\eta(k)) + E_2(\eta(k)) - 2E_3(\eta(k))]\big)\,,\end{aligned}$$

and

$$\begin{aligned}\bar{H}_M^{(2)}(\eta) =& \sum_{k\neq l} \Lambda_2^{(2)}(k,l,k;\eta(k),\eta(l),\eta(k))\\ &+ \sum_{k<l<m} \Lambda_3^{(2)}(k,l,m;\eta(k),\eta(l),\eta(m))\,,\end{aligned}$$

where

$$\begin{aligned}\Lambda_2^{(2)}(k,l,k;\,\eta(k),\eta(l),\eta(k)) = -\frac{\beta}{2}\big(&j_{kkl}^2\,[-E_3(\eta(k))E_1(\eta(l)) + E_2(\eta(k))E_1(\eta(l))\\ &+ E_1(\eta(k))E_2(\eta(l)) - E_3(\eta(l))E_1(\eta(k))\,]),\end{aligned}$$

$$\begin{aligned}\Lambda_3^{(2)}(k,l,m;\,\eta(k),\eta(l),\eta(m)) = \beta\big(&j_{klm}^2\,[E_1(\eta(k))E_1(\eta(m))(1-E_2(\eta(l)))]\\ &+ j_{lmk}^2\,[E_1(\eta(k))E_1(\eta(l))(1-E_2(\eta(m)))]\\ &+ j_{mkl}^2\,[E_1(\eta(m))E_1(\eta(l))(1-E_2(\eta(k)))]\big).\end{aligned}$$

The terms E_i *are defined in* (2.1)–(2.4) *and the quantities* $j_{kl}^1, j_{kl}^2, j_{k_1k_2k_3}^2$ *are defined in* (2.13)–(2.15).

2. *The Gibbs measure is* $\bar{\mu}_{M,\beta}^{(2)}(d\eta) = \frac{1}{\bar{Z}_M^{(2)}} e^{-(\bar{H}_M^{(0)} + \bar{H}_M^{(1)} + \bar{H}_M^{(2)})} \bar{P}_M(d\eta)$.
3. *The relative entropy error is*

$$\frac{1}{N}\mathcal{R}(\bar{\mu}_{M,\beta}^{(2)} | \mu_{N,\beta} \circ \mathbf{F}^{-1}) \sim \mathcal{O}(\epsilon^3)\,.$$

We choose the definition of corrections in such a way that $\bar{H}_M^{(0)}(\eta)$ consists of only two-body interactions, as does $\bar{H}_M^{(1)}(\eta)$, whereas $\bar{H}_M^{(2)}(\eta)$ includes three-body interactions. Note that $\Lambda_2^{(2)}$ is essentially a three-body interaction term even though it involves only two coarse cells. This follows from the graphs in the cluster expansion; see [14, section 2].

The multibody interactions given by $\bar{H}_M^{(2)}(\eta)$ in Scheme 2.2 are also temperature dependent, and hence they are expected to be more important in low temperature

regimes rather than in high temperature regimes. We show in the next section the precise dependence of the correction terms on temperature. Temperature dependence of the corrections has been seen in coarse-graining of polymer chains (see section 6), where most of the schemes do not include the multibody interactions.

The multibody interactions such as the three-body interactions in Scheme 2.2 can be computationally expensive [14]. Hence it is important to understand when the multibody interactions are needed. For example, we show in section 3.2.1 that when coarse-graining smooth long-range potentials with decay the Scheme 2.1 is an accurate approximation and does not require including the multibody interactions. Furthermore, strategies to decrease the computational cost of implementing the multibody interactions are discussed in sections 3.4.1 and 3.4.2.

3. Error quantification and multibody interactions. In this section we analyze the dependence of the coarse-graining error on the detailed characteristics of the interaction potential J. We represent the error as a sum of the error from short-range interactions between coarse cells and the error from long-range interactions of the coarse cells. Considering the coarse-graining error in this way will allow us to control and estimate exactly the error from each piece of the potential based on its behavior.

First, we associate a cutoff distance r_c with a given potential and use this quantity to classify the interactions either as short- or long-range. Thus the error is broken into two pieces as given by the following simple estimate. If $\mathbf{F}(\sigma) = \eta$, then we have

$$\epsilon = \frac{\beta}{N}\left|H_N(\sigma) - \bar{H}_M^{(0)}(\eta)\right| \le e_s + e_l\,, \tag{3.1}$$

where e_s and e_l are the error bounds from coarse-graining short- and long-range interactions, respectively:

$$e_s = \frac{\beta}{N}\sum_k \sum_{\{l\,:\,r_{|k-l|}\le r_c\}} \mathrm{D}_{kl}\,, \quad e_l = \frac{\beta}{N}\sum_k \sum_{\{l\,:\,r_{|k-l|}> r_c\}} \mathrm{D}_{kl}\,,$$

and the total variation of the potential J is

$$\mathrm{D}_{kl} := \sum_{\substack{x\in C_k\,,y\in C_l\\ x\neq y}} |J(x-y) - \bar{J}(k,l)|\,.$$

Thus the choice of the cutoff radius r_c should be such that the coarse-graining error $\epsilon = e_s + e_l$ is minimized. To accomplish this, as e_s and e_l are both controlled by $D_{kl}\,, k, l = 1, \ldots, m$, we observe (with a minor abuse of notation) that

$$\mathrm{D}_{kl} \sim \max_{x\in C_k\,,y\in C_l} |\nabla_{x,y} J(x-y)|\,, k \neq l \quad \text{and} \quad \mathrm{D}_{kk} \sim \sum_{\substack{x\in C_k\,,y\in C_k\\ x\neq y}} |\nabla_{x,y} J(x-y)|. \tag{3.2}$$

Hence controlling norms of the gradient of J will determine if Scheme 2.1 is adequate, i.e., $\epsilon \ll 1$, or if higher-order terms are necessary: in many typical potentials, $\nabla_{x,y} J$ is large when $|x-y|$ is small, while it remains bounded and decays as $|x-y|$ grows. This observation suggests that a suitable coarse-graining strategy would be to employ a higher-order scheme for the error e_s and to use the simple and inexpensive Scheme 2.1 for e_l. We clarify these comments below and in section 3.4 by presenting examples of specific potentials which are of relevance to various applied fields. We identify the error in terms of the parameter ϵ in (2.16) as suggested by (3.1). The detailed calculations are rather straightforward and are omitted.

3.1. Finite-range interactions. A spin at site x interacts with its neighbors which are at most L lattice points away from x. It will be useful to consider the range of the interaction L as a parameter of the model. Then the potential $J(x-y)$ can be taken to have the form

$$J(x-y) = \frac{1}{L^d} V\left(\frac{n}{L}|x-y|\right), \quad x, y \in \Lambda_N, \tag{3.3}$$

where the function $V : (0,1] \to \mathbb{R}$ has a compact support in $[0,1]$. The factor $1/L^d$ in (3.3) is a normalization which ensures that the strength of the potential J is essentially independent of L and $\| J \| \simeq \int |V(r)| dr$.

An example is the piecewise constant potential which is widely used as a benchmark in simulations. Note that even though we present this discussion in dimension $d = 1$, it can be extended to higher dimensions. Suppose that $V(r) = \frac{J_0}{2}$ for $|r| \leq 1$ and is equal to zero otherwise. We define J by (3.3) with the interaction radius L, i.e., $J(x-y) = \frac{J_0}{2L}$ when $n|x-y| \leq L$, $x, y \in \Lambda_N$. Assume that the coarse-graining level is q; then it follows, by simple counting, that the error ϵ is given by

$$\epsilon \equiv \beta \frac{1}{q} \left(\frac{J_0}{4L}(q^2-1) + \frac{J_0}{L}\left(\frac{2q-1}{q} + \frac{q-2}{q^2} \right) \right). \tag{3.4}$$

Similarly, for general potentials of the type (3.3) it is easy to show that [14]

$$|J(x-y) - \bar{J}(k,l)| \leq 2 \frac{q}{L^{d+1}} \|V'\|_\infty; \tag{3.5}$$

thus a similar error representation to (3.4) is true.

The parameter ϵ in (3.4) implies that Scheme 2.1 is expected to work well when $\frac{q}{L} \ll 1$; otherwise Scheme 2.2 would be more suitable. Indeed in Figures 6 and 7 we demonstrate the influence of the multibody interactions included in Scheme 2.2 in the case when $\frac{q}{L} \sim \mathcal{O}(1)$.

3.2. Kac-type interactions. In this case we assume that a spin interacts with all spins, i.e., $L = n$ in the above case of finite-range interactions, and the potential is given by

$$J(x-y) = \frac{1}{N} V\left(|x-y|\right), \quad x, y \in \Lambda_N \,. \tag{3.6}$$

In this class of examples we are particularly interested in the role of the singularity and the decay of the potential. For this reason we consider two classes of examples.

3.2.1. Power–law-type potentials. Assume that J is given by (3.6) and $V \in C^1(0,\infty)$ satisfies

$$|V(r)| \leq \frac{K}{r^\alpha}, \quad |V'(r)| \leq \frac{K}{r^{\alpha+1}} \quad \text{for } r > r_c. \tag{3.7}$$

Then we have

$$|\bar{J}(k,l)| \leq \frac{K}{N} \frac{1}{(r_{|k-l|})^\alpha} \qquad \forall\, k, l \text{ such that } r_{|k-l|} > r_c \,. \tag{3.8}$$

And if $x \in C_k$ and $y \in C_l$, then

$$|J(x,y) - \bar{J}(k,l)| \leq \frac{2K\alpha\sqrt{d}}{q^d m^{d+1}} \frac{1}{(r_{|k-l|})^{\alpha+1}} \quad \forall\ k, l \text{ such that } r_{|k-l|} > r_c. \tag{3.9}$$

Note the improved decay in (3.9); this fact will be used in a crucial way in section 3.4.1. Based on the above estimates we obtain

$$\epsilon = e_s + e_l \leq e_s + C\beta\frac{1}{m}, \tag{3.10}$$

where e_s and e_l represent the error made by coarse-graining of the short-range and long-range interactions given by (3.1). The estimate suggests that if the coarse grid is such that both e_l and e_s are small (i.e., m is large enough), then Scheme 2.1 will perform well; see Figures 2 and 3. Furthermore, it also suggests that using a potential-splitting method when $e_l \ll 1$ and $e_s \sim \mathcal{O}(1)$ can provide a satisfactory approximation; see section 3.4.2 below.

3.2.2. Potentials with locally integrable gradient. We assume that the potential V satisfies the condition $r^{d-1}V'(r) \in L^1_{loc}(0,\infty)$. Such potentials include Coulomb interactions in particle simulations where the interactions are inversely proportional to the distance in $\mathbb{R}^3$ [22]. Another example is the description of two-dimensional turbulence where the interactions are proportional to the logarithm of the distance between two vortices located at the sites x and y, respectively [24].

Assuming that J is given by (3.3), $V(r) \in C^1(0,\infty)$, and $r^{d-1}V'(r) \in L^1_{loc}$, we have for $x \in C_k$ and $y \in C_l$

$$|J(x,y) - \bar{J}(k,l)| \leq \frac{1}{N}\|r^{d-1}V'\|_{L^1(r_{kl}-\frac{\sqrt{d}}{m}, r_{kl}+\frac{\sqrt{d}}{m})}, \tag{3.11}$$

and consequently the parameter ϵ is bounded by

$$\epsilon \leq \beta\frac{C}{m}\|r^{d-1}V'(r)\|_{L^1_{loc}}. \tag{3.12}$$

Hence ϵ is small, provided that we have corresponding conditions on the coarse-grained grid size $\frac{1}{m}$ and the radial norm of V'. In this case Scheme 2.1 is expected to perform well. We can also obtain bounds similar to (3.11) in L^∞, for $k \neq l$, similarly to (3.5).

Beyond the aforementioned examples, we will also discuss in section 5 simulations with competing short- and long-range potentials. This class of interactions is common both in lattice and off-lattice models, e.g., in epitaxial growth processes and in polymers. A typical potential of this kind arising in off-lattice models is the Lennard-Jones interaction.

3.3. Applicability to other models. The error analysis in the previous examples allows us to derive suitable conditions under which the coarse-graining schemes work well, and conversely it suggests when they are not expected to perform adequately. For instance, (3.4) or (3.5) implies that the schemes perform well for long-range interactions ($L \gg 1$), even when the temperature T is not necessarily high. In contrast, for short-range potentials, e.g., $L = 1$, the coarse-graining schemes provide a good numerical approximation only at relatively high temperatures. The same issues related to the coarse-graining of short-range interactions arise in (3.10). These difficulties are intuitively obvious, for instance, in systems that exhibit microstructure at the smallest scales such as the nearest neighbor antiferromagnetic Ising model, where (1.3) is expected to be a particularly poor approximation of the microscopic model. We refer the reader to [14] (Figures 1 and 2) and [12] (Figures 4 and 5) for several related simulations demonstrating these shortcomings.

Nevertheless, coarse-graining schemes can be used even in these systems by following a different, hierarchical approach. In [12] we used a posteriori error estimates

(obtained through the cluster expansions), in order to adaptively construct phase diagrams of antiferromagnetic systems, as well as of model systems with combined short- and long-range interactions proposed in [8]. These two examples were selected as numerical benchmarks because their phase diagrams are known analytically and since coarse-graining was not expected to work outright. For example, in the antiferromagnetic case the a posteriori error estimates can determine on-the-fly a region of external fields where it is possible to simulate cheaply and accurately with a progressively higher level of coarse-graining q as we increase the external field. On the other hand, at lower external fields microstructure is typical and the coarse-graining based on (1.3) yields a high a posteriori error; in this case the hierarchy of coarse-grained resolutions q adaptively adjusts to a full microscopic simulation $q = 1$ [12]. Overall the coarse-graining schemes permit us to construct numerically the phase diagram in a computationally efficient manner, which necessitates the use of microscopic simulation in only a part of the parameter domain.

Finally, based on a closer inspection of the coarse-graining strategy outlined in section 2.2, it is expected that lattice systems with more general order parameters, e.g., Potts and Heisenberg models, will have similar coarse-graining error estimates and cluster expansions with analogous limitations to the ones encountered in the Ising systems. On the other hand, the coarse-graining of off-lattice systems has some unique challenges and is discussed separately in section 6.

3.4. Efficient implementation of multibody interactions. To address the computational complexity associated with implementing Scheme 2.2, we employ the error estimates in the previous subsections in order to show that multibody interactions can be compressed following two different and complementary strategies.

3.4.1. Compression through truncations. From the computational point of view, calculating the three-body corrections, i.e., $\bar{H}_M^{(2)}(\eta)$, can be quite expensive, depending on the number of nonzero terms in j^2_{klm}. In this direction, we recall that in analogy to (3.2) we have

(3.13)
$$j^1_{kl},\, j^2_{kl},\, j^2_{klm} \sim \max_{x\in C_k\,, y\in C_l} \left|\nabla_{x,y} J(x-y)\right|, \max_{x\in C_k\,, y\in C_m} \left|\nabla_{x,y} J(x-y)\right|, \quad k\neq l, m\,.$$

These bounds imply that for large $r_{|k-l|}, r_{|k-m|}$ the terms j^1_{kl}, j^2_{kl}, j^2_{klm} decay faster than $\bar{J}(k,l), \bar{J}(k,m)$ (see the example in section 3.2.1); hence they can be suitably truncated within a given tolerance.

3.4.2. Compression through potential-splitting. Another approach to further increase the computational efficiency of the schemes presented in section 2.4 is to decompose the coarse-graining of the interaction potential based on the size of the error in (3.1). Indeed these estimates suggest a natural way to split the potential into a short-range piece with possible singularities and a locally integrable (or smooth) long-range decaying component such as the ones considered, for instance, in (3.10):

$$J(x,y) = J_s(x,y) + J_l(x,y)\,.$$

In this way the computational expense of Scheme 2.2 can be decreased by implementing this higher-order scheme for the short-range piece $J_s(x,y)$ alone, while using the inexpensive 2nd-order Scheme 2.1 for the long-range piece $J_l(x,y)$. The latter is sufficient, provided that m is large enough; see, for instance, (3.10) or (3.12). This

approach is also suitable in the case when the interactions are combinations of possibly competing short- and long-range interactions. We refer the reader to the example considered in section 5.2 as well as in the simulations depicted in Figure 4.

4. Coarse-grained stochastic dynamics. In this section we extend our analysis in order to construct efficient and accurate coarse-graining methods for the approximation of not only the equilibrium invariant measure $\mu_{N,\beta}$ but also for the approximation of the measure on the path space. We start with a brief description of the microscopic and the coarse-grained lattice dynamics. We refer the reader to Figure 1 for a schematic description of the dynamics.

4.1. Microscopic MC algorithms. The sampling algorithm for the microscopic lattice system is given in terms of a continuous-time jump Markov process $\{\sigma_t\}_{t\geq 0}$. The generator of this stochastic process $\mathcal{L}_N$ is given by

$$(\mathcal{L}_N f)(\sigma) = \sum_{x\in\Lambda_N} c(x,\sigma)\,(f(\sigma^x) - f(\sigma)) \tag{4.1}$$

for a bounded test function $f \in L^\infty(\mathcal{S}_N)$. Here $c(x,\sigma)$ denotes the rate of the process and σ^x represents the configuration after a flip at x.

In general, for sampling the equilibrium Gibbs measure a wide class of Metropolis-type algorithms is available. The kinetic Monte Carlo (KMC) methods [3] represent a class of such methods that are also suitable for simulating nonequilibrium processes. An example of dynamics widely used for simulations of *interacting* particles on a lattice is known as *Arrhenius dynamics*. The rates are usually derived from the transition-state theory or obtained from MD simulations. The Arrhenius spin-flip rate is defined as

$$c(x,\sigma) = d_0\sigma(x) + d_0(1-\sigma(x))e^{-\beta U(x,\sigma)}\,, \tag{4.2}$$

where $U(x,\sigma)$ is the potential which is given by

$$U(x,\sigma) = \sum_{y\in\Lambda_N\, y\neq x} J(x-y)\sigma(y)\,. \tag{4.3}$$

It can be easily verified that the Arrhenius rate defined in (4.2) satisfies the detailed balance condition

$$c(x,\sigma)e^{-\beta H(\sigma)} = c(x,\sigma^x)e^{-\beta H(\sigma^x)}\,, \tag{4.4}$$

which in turn guarantees that the invariant measure of this Markov process is the Gibbs measure (1.2).

4.2. Coarse-grained MC algorithms. Given the Markov process $(\{\sigma_t\}_{t\geq 0}, \mathcal{L})$ with the generator $\mathcal{L}$ we obtain a coarse-grained process $\{\mathbf{F}(\sigma_t)\}_{t\geq 0}$. The fact that the process $\{\mathbf{F}(\sigma_t)\}_{t\geq 0}$, in general, is not a Markov process poses a significant difficulty mathematically and computationally in studying this process. One way to overcome this difficulty in computations is by deriving an approximating coarse-grained Markov process $(\{\eta_t\}_{t\geq 0}, \bar{\mathcal{L}}^c)$ which can be easily implemented once its generator is given explicitly.

For the purpose of sampling the coarse-grained Gibbs measure given by $\bar{\mu}^{(0)}_{M,\beta}(\eta)$ we consider a Markov birth-death process with the generator

$$\bar{\mathcal{L}}^c g(\eta) = \sum_{k\in\bar{\Lambda}_M} \bar{c}_b(k,\eta)\,[g(\eta+\delta_k) - g(\eta)] + \sum_{k\in\bar{\Lambda}_M} \bar{c}_d(k,\eta)\,[g(\eta-\delta_k) - g(\eta)]\,, \tag{4.5}$$

where the rates $\bar{c}_b(k,\eta)$, $\bar{c}_d(k,\eta)$ correspond to adding a particle (birth) and removing a particle (death) from the coarse cell.

In the case of nonequilibrium dynamics like the *Arrhenius dynamics* the strategy is to derive the rates $\bar{c}_b(k,\eta)$, $\bar{c}_d(k,\eta)$ which have the same form as the microscopic rates for *Arrhenius dynamics* given by (4.2). Deriving the rates in this way allows us not only to approximate the measure $\mu_{N,\beta}(\sigma)$ but also gives an approximation of the measure on the path space. The approximate rates were derived in [9, 10] and are given by

$$\bar{c}_a(k,\eta) = d_0(q-\eta(k))\,, \qquad \bar{c}_d(k,\eta) = d_0\eta(k)e^{-\beta(\bar{U}^{(0)}(k,\eta)}\,. \tag{4.6}$$

The new interaction potential $\bar{U}^{(0)}(\eta)$ represents an approximation of the original interaction potential $U(\sigma)$ and is defined as

$$\bar{U}^{(0)}(k,\eta) = \sum_{\substack{l\in\bar{\Lambda}_M\\ l\neq k}} \bar{J}(l,k)\eta(l) + \bar{J}(0,0)(\eta(k)-1)\,. \tag{4.7}$$

We note that by definition $\bar{U}^{(0)}(k,\eta)$ satisfies the following condition:

$$\bar{U}^{(0)}(k,\eta) = \bar{H}_M^{(0)}(\eta) - \bar{H}_M^{(0)}(\eta-\delta_k)\,.$$

As shown in [9] this property is sufficient for the detailed balance condition with respect to the coarse-grained measure $\bar{\mu}_{M,\beta}^{(0)}$ in Scheme 2.1 to hold. In other words we have

$$\bar{c}_a(k,\eta)\ e^{-\beta\bar{H}_M^{(0)}(\eta)} = \bar{c}_d(k,\eta+\delta_k)\ e^{-\beta\bar{H}_M^{(0)}(\eta+\delta_k)}\,.$$

In [11] an error estimate between the time-dependent probability, $\mu_{m,q,\beta}(t)$, and the exact projection on the coarse variables of the microscopic probability, $\mu_{N,\beta}\circ\mathbf{F}^{-1}(t)$, was obtained. The error is calculated on arbitrary coarse observable ϕ, which necessitates the use of a weak convergence framework. More specifically, in [11] the 2nd-order accuracy of the process (4.6) in terms of the parameter ϵ in (2.16) was established:

$$|\mathbb{E}[\psi(\mathbf{F}\sigma_T)] - \mathbb{E}[\psi(\eta_T)]| \le C_T\epsilon^2\,, \quad t\in[0,T]\,, \tag{4.8}$$

where the constant C_T is independent of the system-size N. Similar estimates were also obtained in [16], where the time-dependent error estimate was given in terms of the relative entropy. We also refer the reader to [15] for a coarse-grained Langevin-type approximation to KMC and related time-dependent estimates in the weak topology.

The strategy that was used to derive the approximating process $(\{\eta_t\}_{t\ge0},\bar{\mathcal{L}}^c)$ suggests a straightforward extension to obtain higher-order approximations of the microscopic dynamics. Such dynamics are defined in the terms of higher-order coarse rates $\bar{c}_a^{(\alpha)}(k,\eta)$, $\bar{c}_d^{(\alpha)}(k,\eta)$, and they need to satisfy the detailed balance for $\bar{\mu}_{M,\beta}^{(\alpha)}$ in order to ensure a similar behavior to the dynamics (4.6). For such higher-order *Arrhenius dynamics* we define the new coarse-grained rates as

$$\bar{c}_a^{(\alpha)}(k,\eta) = d_0(q-\eta(k))\,, \qquad \bar{c}_d^{(\alpha)}(k,\eta) = d_0\eta(k)e^{-\beta\left(\bar{U}^{(0)}(\eta)+\cdots+U^{(\alpha)}(\eta)\right)}\,, \tag{4.9}$$

where $\alpha = 1,2,\ldots$. The detailed balance condition is then in the form

$$\bar{c}_a^{(\alpha)}(k,\eta)\ e^{-\beta(\bar{H}_M^{(0)}(\eta)+\cdots+\bar{H}^{(\alpha)}(\eta))} = \bar{c}_d^{(\alpha)}(k,\eta+\delta_k)\ e^{-\beta(\bar{H}_M^{(0)}(\eta+\delta_k)+\cdots+\bar{H}^{(\alpha)}(\eta+\delta_k))}\,. \tag{4.10}$$

The new interaction potential $\bar{U}^{(0)}(\eta) + \cdots + U^{(\alpha)}(\eta)$ represents the higher-order approximation of the original interaction $U(\sigma)$. In order to satisfy the detailed balance condition (4.4) for the higher-order coarse-grained Gibbs measure we define higher-order coarse potentials by

$$\bar{U}^{(\alpha)}(\eta) := \bar{H}^{(\alpha)}(\eta) - \bar{H}^{(\alpha)}(\eta - \delta_k)\,, \tag{4.11}$$

where $\alpha = 0, 1, \ldots$. Note that just as in (4.7) calculating $\bar{U}^{(\alpha)}(\eta)$ involves a local difference and does not require calculating the complete Hamiltonian. Specifically for Scheme 2.2 the higher-order potentials are given by

$$\begin{aligned}
\bar{U}^{(1)}(k,\eta) = & \sum_{\substack{l\in\bar{\Lambda}_M\\ l\neq k}} \left[\Lambda_2^{(1)}(k,l;\,\eta_k,\eta_l) - \Lambda_2^{(1)}(k,l;\,\eta_k-1,\eta_l)\right] \\
& + \Lambda_1^{(1)}(k;\,\eta_k) - \Lambda_1^{(1)}(k;\,\eta_k-1), \\
\bar{U}^{(2)}(k,\eta) = & \sum_{\substack{l\in\bar{\Lambda}_M\\ l\neq k}} \left[\Lambda_2^{(2)}(k,l,k;\,\eta_k,\eta_l,\eta_k) - \Lambda_2^{(2)}(k,l,k;\,\eta_k-1,\eta_l,\eta_k-1)\right] \\
& + \sum_{l<m} \left[\Lambda_3^{(2)}(k,l,m;\,\eta_k,\eta_l,\eta_m) - \Lambda_3^{(2)}(k,l,m;\,\eta_k-1,\eta_l,\eta_m)\right].
\end{aligned} \tag{4.12}$$

Note that these calculations can also be simplified by truncating as in section 3.4.1 or by splitting the potential as in section 3.4.2.

Finally, we remark on the time-dependent error analysis for the new process defined in terms of the rates (4.9). These new rates are perturbations of (4.6); hence similar time-dependent estimates to [16, 11] hold. In fact, in analogy to these results, e.g., (4.8), we would expect that the (weak topology) estimate between the time-dependent probability $\mu^{(\alpha)}_{m,q,\beta}(t)$ and the exact projection on the coarse variables of the microscopic probability $\mu_{N,\beta}\circ\mathbf{F}^{-1}(t)$ could be of order $\mathcal{O}_T(\epsilon^{\alpha+1})$. However, we do not have a proof of this conjecture at the present time. Nevertheless, the comparative simulations in Figures 6, 7, and 8 and Table 2 based on (4.9) suggest a higher-order accuracy than the dynamics based on the rates (4.6).

5. Computational algorithms and numerical experiments. The 2nd-order coarse-grained algorithm as described in Scheme 2.1 has been extensively studied in previous works, e.g., [10, 9, 11]; there it has been demonstrated, both rigorously and computationally, that it performs well in high temperature regimes or when long-range interactions are involved, in the latter case even when phase transitions are present. However, coarse-grained Monte Carlo (CGMC) simulations for lattice systems with short- or intermediate-range potentials using Scheme 2.1 do not accurately capture hysteresis and critical behavior [9]. In earlier benchmark simulations using the 3rd-order coarse-graining Scheme 2.2 for piecewise constant potentials (see section 3.1), it was shown that such an error was substantially reduced [14, 12].

In the simulations discussed here we present numerical experiments based on spin-flip Arrhenius dynamics, using more realistic potentials such as the ones in sections 3.2.1 and 3.2.2. In particular, we emphasize simulations involving dynamics, rare events, and complex critical behavior not addressed in our earlier work. Furthermore, based on the error analysis of section 3 we assess numerically the importance of multibody interactions. Finally, numerical results show the effectiveness of the potential-splitting method, discussed in section 3.4.2.

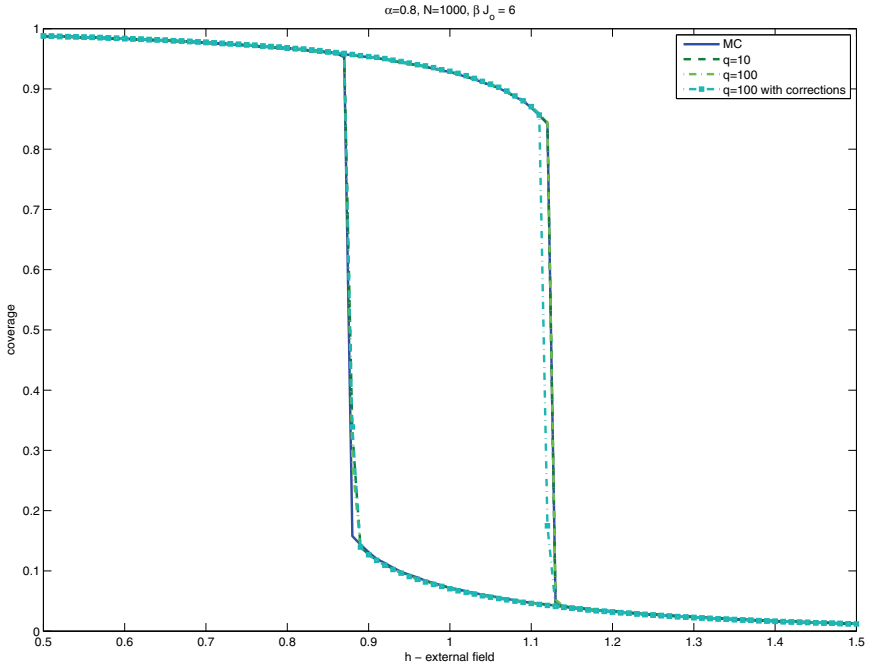

FIG. 2. *Comparison of different fully resolved (MC) simulations with coarse-grained* $q = 10$*, coarse-grained* $q = 100$*, and coarse-grained* $q = 100$ *with corrections. The potential here is the decaying potential* (5.1) *with* $\alpha = 0.8$*. We observe that corrections due to three-body terms have minimal impact, as Scheme* 2.1 *is already performing well for less singular potentials.*

5.1. Kac potentials with singularities. In this set of simulations we use examples of different long-range potentials as in (3.6), where the function V has an algebraic decay (see inset in Figure 2):

$$V(r) = \frac{K}{|r|^\alpha} \quad \text{if } |r| > 0; \tag{5.1}$$

and the constant K is such that the total mass is kept fixed:

$$\frac{J_0}{2} = \frac{1}{N}\sum_{i=1}^{N} V\left(\frac{i}{N}\right) = KN^{\alpha-1}\sum_{i=1}^{N}\frac{1}{i^\alpha}\,.$$

We compute isotherms similarly to the natural parameter continuation, i.e., we trace the total coverage $N^{-1}\sum_{x\in\Lambda_N}\sigma(x)$, while changing the external field h, first upon increasing the field h from low values and then decreasing it from high values. In particular, we look at the two exponent cases, $\alpha = 0.8$ and $\alpha = 1.5$, for which we study their respective hysteresis behaviors. In the numerical tests presented here we demonstrate that the corrections derived improve this behavior even in the case of high coarse-graining ratio q. The sampling of the equilibrium measure is done by using microscopic and coarse-grained Arrhenius dynamics discussed in section 4.

It is observed in the numerical experiments that the multibody terms which are given by j^2_{klm} are more important for higher values of α; this observation is in agreement with the estimates in (3.13) and (3.9), where higher values of α yield larger errors for Scheme 2.1, if k, l, m are suitably close together. For example, in the case

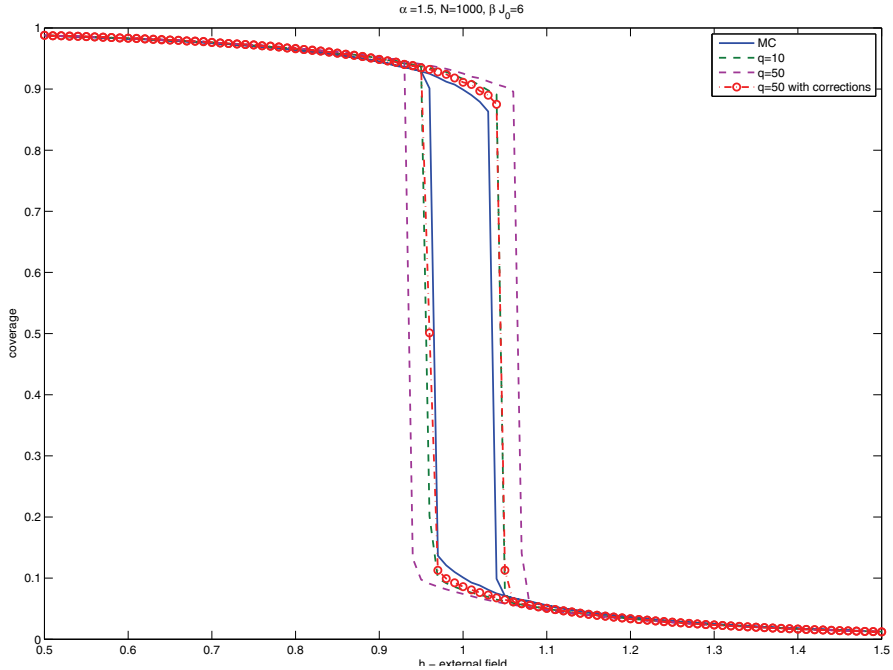

FIG. 3. *Comparison of different fully resolved (MC) simulations with coarse-grained* $q = 10$*, coarse-grained* $q = 50$*, coarse-grained* $q = 50$ *with corrections, and coarse-grained* $q = 200$ *with corrections. The potential here is the decaying potential* (5.1) *with* $\alpha = 1.5$*. The results from the* 3*rd-order Scheme* 2.2 *with* $q = 50$ *are identical to the results from the* 2*nd-order Scheme* 2.1 *with* $q = 10$*.*

when $\alpha = 0.8$ (see Figure 2), the 2nd-order coarse-graining Scheme 2.1 provides very good approximation even for high levels of coarse-graining (large q), whereas, in the case $\alpha = 1.5$ (see Figure 3), the 2nd-order coarse-graining Scheme 2.1 is not sufficient. For larger values of q the 3rd-order Scheme 2.2 appears to be a much better approximation than the 2nd-order coarse-graining Scheme 2.1 as q increases. Notice that the results from the 3rd-order Scheme 2.2 with $q = 50$ are identical to the results from the 2nd-order Scheme 2.1 with $q = 10$. Not shown here, the results for $\alpha = 1.5$ obtained by the 3rd-order Scheme 2.2 with $q = 200$ were much better when compared to the results from the 2nd-order Scheme 2.1 with $q = 50$.

5.2. Competing short-/long-range interactions and potential-splitting. In this example we consider a combination of short-range, repulsive, and long-range attractive interactions. These types of potentials arise in numerous applications modeled by lattice or off-lattice systems in fields, such as epitaxial growth or macromolecular systems. The potential used in the tests is given by

$$J(x-y) = \begin{cases} \dfrac{1}{3}\left(\dfrac{a}{|x-y|} - \dfrac{a^2}{|x-y|^2}\right), & |x-y| \le a, \\ K_N\left(\dfrac{a}{|x-y|} - \dfrac{a^2}{|x-y|^2}\right), & |x-y| > a, \end{cases} \qquad x, y \in \Lambda_N, \tag{5.2}$$

where K_N is such that $\frac{J_0}{2} = \sum_{i=1}^{N/2} J(i)$ is fixed and $a = \frac{3}{N}$. This interaction resembles an off-lattice Lennard-Jones potential, where the parameter a regulates the length of

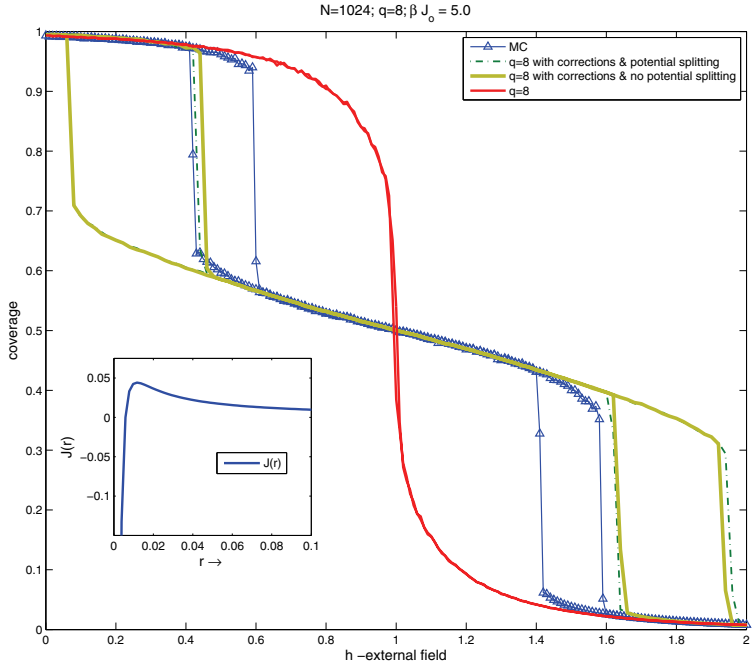

FIG. 4. *Comparison of hysteresis using the potential* (5.2) *of the microscopic process (MC) with the coarse-grained process* $q = 8$*, the coarse-grained process* $q = 8$ *with corrections using the full potential, and the coarse-grained process* $q = 8$ *with corrections using the split potential for* $\beta J_0 = 5.0$*. We note that with corrections the antiferromagentic behavior is accurately predicted, while the double hysteresis width is not estimated properly. The inset shows the potential given by* (5.2).

the short-range repulsive particle interactions (here it is three neighbors). However, in the lattice case we insert in the long-range piece a rescaling by K_N (where $K_N \to \infty$ as $N \to \infty$), in order to keep the total strength of the interaction J_0 fixed as the lattice size $N \to \infty$, ensuring a nontrivial thermodynamic limit. In fact, in our microscopic simulations we have also tested for finite-size effects by simulating for various lattice sizes N. Then, the microscopic system ($q = 1$) exhibits, at low temperature (see Figure 5), a complex hysteresis diagram with a double hysteresis separated by an antiferromagnetic region.

The coarse-graining Scheme 2.1 fails to capture this behavior, while Scheme 2.2 does a much better job resolving the antiferromagnetic region. Furthermore, it predicts qualitatively the double hysteresis, albeit in a shifted location. In Figure 5 we present the hysteresis using the potential given by (5.2) for the microscopic process, the coarse-grained process with $q = 8$, and the coarse-grained process with $q = 8$ and corrections. We remark that similar results hold for $q = 16$, while for $q = 32$ the system is (over-)coarse-grained, especially the repulsive short-range interactions. This behavior is expected according to the estimates in sections 3.2.1 and 3.4.2.

Implementing the 3rd-order scheme requires dense matrix-vector multiplication in the evaluations of $\bar{U}^{(2)}$; for example, j^2_{klm} is a matrix of size 128×128 in the example presented. To overcome this problem, as we discussed in section 3.4.2 we break up the potential into a short-range piece and a smooth long-range piece with $r_c = 16$. This is possible since the smoothness of the long-range piece implies that the error from coarse-graining is small; see (3.2). In Figure 4 we present the hysteresis diagram using

the potential-splitting and applying Scheme 2.2 just for the short-range piece and Scheme 2.1 for the long-range piece. It is observed that the predictions of hysteresis using potential-splitting are essentially identical to the results from simulations when using the full potential.

This last example demonstrates that appropriately decomposing the potential can provide an efficient way of including the multibody terms and reduce the computational complexity of the multibody terms. A CPU time comparison between direct numerical simulations ($q = 1$) and the different coarse-graining schemes and their implementations is shown in Table 1. The case shown here is the calculation of the hysteresis diagram, Figure 4. The potential-splitting ends up reducing the computational cost of Scheme 2.2 to the level of the much less accurate Scheme 2.1.

TABLE 1
CPU cost comparisons of different CG algorithms for (5.2).

$N = 1000$, $\beta J_0 = 6.0$

Process	CPU (secs)
$q = 1$ (no coarse-graining)	322192.06
$q = 8$	5232.62
$q = 8c$ (no splitting)	69473.09
$q = 8c$ (splitting)	6900.72

In Figure 5 we depict the hysteresis results in the same setup as in Figure 4 except at higher temperatures. We observe that the accuracy of Scheme 2.1 as well as Scheme 2.2 is better at higher temperatures. This is expected because the multibody interactions are proportional to β^2, which results in smaller, and hence unnecessary, corrections at higher temperatures.

In conclusion, we observe by comparing Figures 4 and 5 that at low temperatures, even Scheme 2.2 can be insufficient to predict quantitatively the hysteresis diagram. Another perspective, also based on the decomposition in section 3.4.2, is presented in the forthcoming [13], which is designed specifically for systems with combined short- and long-range interactions such as (5.2). The principal idea there is to build a better initial guess than (1.5) for the cluster expansion (1.7). For this purpose we introduce a different prior P_N which already includes *multibody* coarse cell correlations, associated with the short-range interactions.

5.3. Multibody terms and autocorrelations. In Figure 6 we show the impact of the corrections on the dynamics and the fluctuations of the coarse-grained process $\{\eta_t\}$ by comparing autocorrelations of the microscopic and coarse-grained simulations. The potential used here is piecewise constant with an interaction radius $L = 100$, as discussed in section 3.1. The temperature is such that $\beta J_0 = 4.35$. We choose this value of β, as it is close to the mean field critical temperature for such long-range systems. Thus there is enough noise in the system to generate short jumps between the metastable states; see the inset of Figure 6.

In the autocorrelation comparisons for the different coarse-graining schemes, we study the stationary time series of the total coverage $X(t) = \sum_{x\in\Lambda_N} \sigma_t(x)$; the autocorrelation of the time series $\{X_t\}$ as a function of the lag τ is defined as

$$\gamma(h) = \frac{\mathbb{E}[(X_{t+\tau} - \nu)(X_t - \nu)]}{\mathbb{E}[(X_t - \nu)^2]},$$

where $\nu = \mathbb{E}[X_t]$ and $\{X_t\}$ is assumed to be a stationary time series. Figure 6 demonstrates that for systems with long-range interactions the multibody terms in the

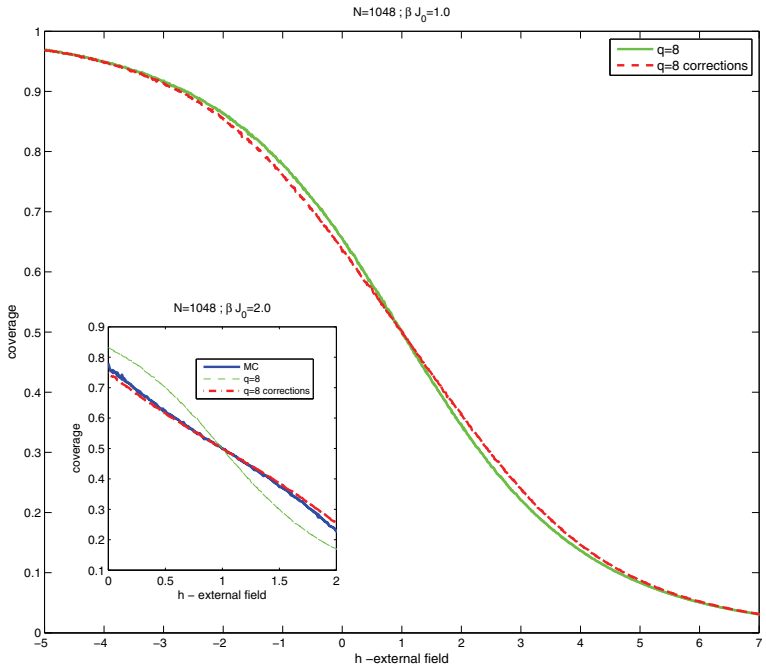

FIG. 5. *Comparison of hysteresis for the potential* (5.2) *at higher temperatures than Figure* 4*: we compare the microscopic process (MC) with the coarse-grained process* $q = 8$ *and the coarse-grained process* $q = 8$ *with corrections for* $\beta J_0 = 1.0$*. The inset is the comparison for* $\beta J_0 = 2.0$*; we note that Scheme* 2.2 *is more appropriate at lower temperatures.*

higher-order coarse-graining schemes are important for approximating the correct dynamical behavior and the random fluctuations of the microscopic process.

5.4. Switching times and phase transitions. We use the coarse-graining schemes described and analyzed in the previous sections for efficient simulations in the spin systems that undergo phase transitions. Within the context of spin-flip dynamics a typical example is nucleation of spatial regions of a new phase or a transition from one phase (all spins equal to zero) to another (all spins equal to one). In such simulations the emphasis is on the pathwise properties of the coarse-grained process so that the switching mechanism is simulated efficiently while approximation errors are controlled. We compare simulations on the microscopic level with those performed on different levels of coarse-graining hierarchy parametrized by q. A quantity of interest that is calculated is the mean time $\bar{\tau}_T = \mathbb{E}[\tau_T]$, which is defined as the time until the coverage reaches a predetermined threshold C^+ in its phase transition regime. The random exit time is defined as $\tau_T = \inf\{t > 0 \,|\, c_t \geq C^+\}$. We estimate the microscopic probability distributions ρ_τ and coarse-grained ρ_τ^q from the simulations. We record a phase transition at the time τ_T when the total coverage X_t defined in the previous section exceeds the threshold value $C^+ = 0.9$. The potential used in the simulations is a piecewise potential with the interaction radius $L = 100$ and $\beta J_0 = 6.0$. Note that $\beta J_0 = 6$, which is above the critical value of $\beta_c J_0 = 4.0$, corresponds to a bistable regime where two phases can coexist. Random fluctuations allow for transitions between the two equilibrium states. In Table 2 we look at a relative error of the mean exit time $\bar{\tau}_T = \mathbb{E}[\tau_T]$ for different levels of coarse-graining, and we observe that the relative error from Scheme 2.1 increases with the size of the coarse-graining. In

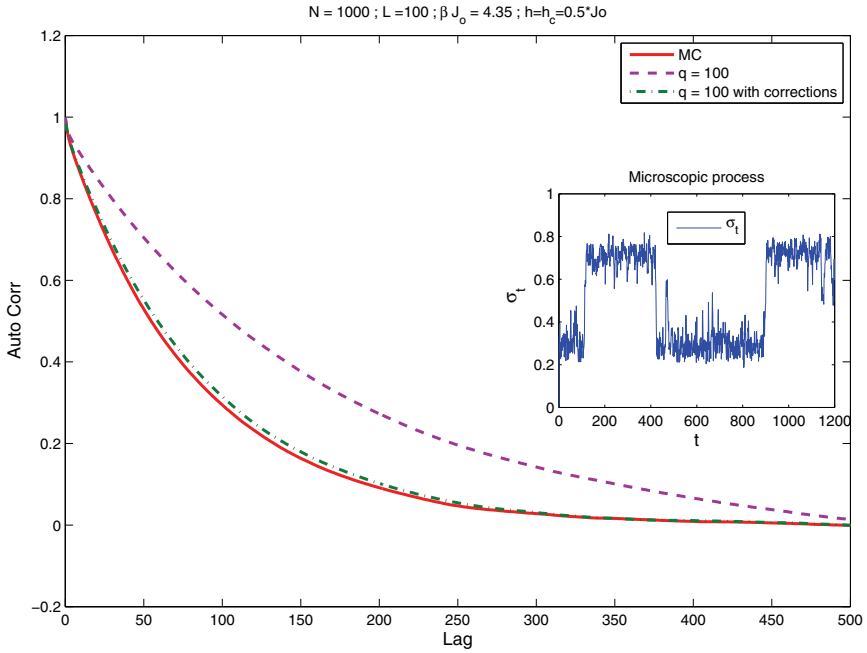

FIG. 6. *Autocorrelation of the time series for the cases fully resolved $q = 1$ (MC), coarse-grained $q = 100$, and coarse-grained with corrections $q = 100$. The potential is piecewise constant with interaction range $L = 100$ and $\beta J_0 = 4.35$. A typical time series is shown in the inset.*

TABLE 2

Approximation of $\bar{\tau}_T$, $\|\rho_\tau^q - \rho_\tau\|_{L^1}$, and the relative error. Measurements based on averaging over 10000 independent realizations for each q.

$N = 1000$, $\beta J_0 = 6.0$, $h = 0.4406$

CGMC without corrections

L	q	$\bar{\tau}_T$	$\|\rho_\tau^q - \rho_\tau\|_{L^1}$	Rel. err.
100	1	486.9	0	0
100	10	491.7	0.0022	1.16%
100	20	503.9	0.0025	3.68%
100	25	511.7	0.0032	5.27%
100	50	584.1	0.0074	20.17%
100	100	980.9	0.0246	101.82%

CGMC with corrections

L	q	$\bar{\tau}_T$	$\|\rho_\tau^q - \rho_\tau\|_{L^1}$	Rel. err.
100	50	480.8	0.0025	1.08%
100	100	479.0	0.0028	1.45%

Table 2 we also present the results from the simulations using Scheme 2.2 and observe that even at high levels of coarse-graining in the 3rd-order scheme the relative error of the mean exit time is very small. In Figure 7 we plot approximations of the probability density functions (PDFs) of τ_T and compare them to the microscopic PDF for different values of coarse-graining q and the respective corrections. We observe that including the multibody interactions improves the approximation of the PDF substantially. In Table 3 and Figure 8 we present results from simulations that were carried out under the same conditions but at a different (lower) temperature. The results for the higher-

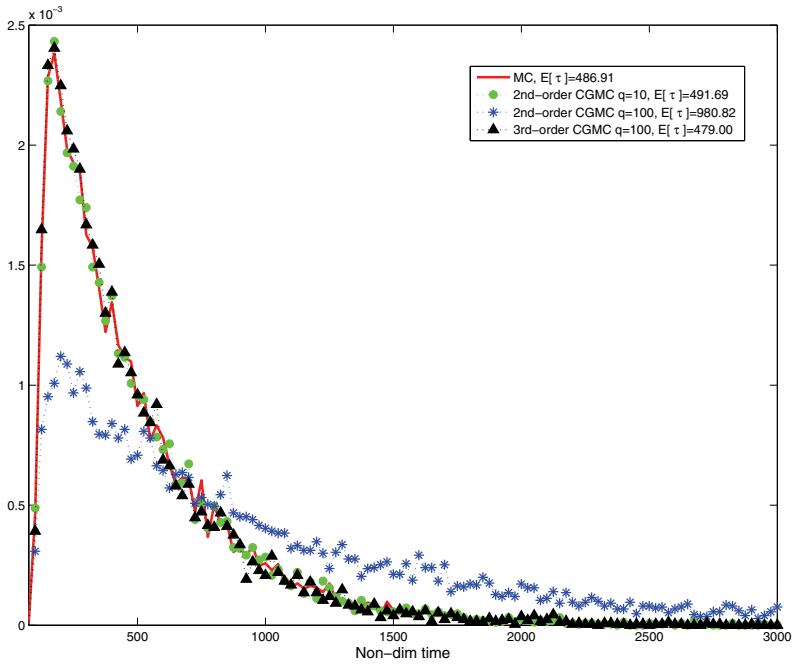

FIG. 7. *PDF: comparisons between different coarse-graining levels q. The estimated mean times for each PDF are shown in the legend. All PDFs are comprised of* 10000 *samples, and the histogram is approximated by* 200 *bins. The potential is a piecewise constant potential with the interaction range $L = 100$ and $\beta J_0 = 5.0$.*

order scheme qualitatively show an improvement. However, the error increases in the case of lower temperature. This is expected because ϵ, defined in (3.4), depends on the inverse temperature β.

TABLE 3

Approximation of $\bar{\tau}_T$, $\|\rho_\tau^q - \rho_\tau\|_{L^1}$, and the relative error. Measurements based on averaging over 10000 *independent realizations for each q.*

$N = 1000$, $\beta J_0 = 8.0$, $h = 0.38375$

CGMC without corrections

L	q	$\bar{\tau}_T$	$\|\rho_\tau^q - \rho_\tau\|_{L^1}$	Rel. err.
100	1	367.9	0	0
100	10	379.4	0.0032	3.13%
100	20	398.3	0.0038	8.25%
100	25	416.1	0.0046	13.09%
100	50	569.4	0.0131	54.78%
100	100	1482.23	0.0416	302.9%

CGMC with corrections

L	q	$\bar{\tau}_T$	$\|\rho_\tau^q - \rho_\tau\|_{L^1}$	Rel. err.
100	50	335.9	0.0042	8.68%
100	100	290.6	0.0072	21.00%

6. Connections to coarse-graining of polymer chains: The McCoy–Curro scheme. So far we have studied coarse-graining of lattice systems with a focus on understanding the error from coarse-graining and developing a methodol-

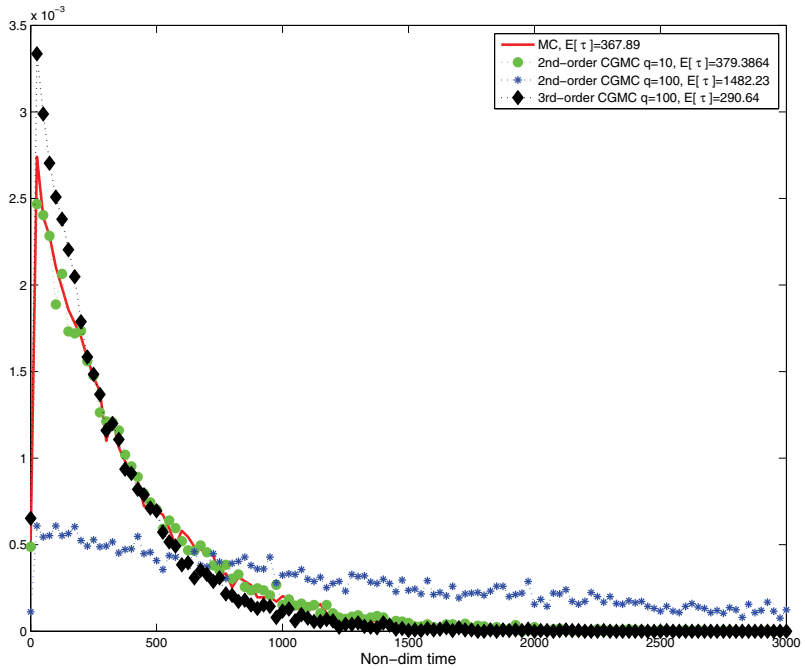

FIG. 8. *PDF: comparisons between different coarse-graining levels q. The estimated mean times for each PDF are shown in the legend. All PDFs are comprised of* 10000 *samples, and the histogram is approximated by* 200 *bins. The potential is a piecewise constant potential with the interaction range* $L = 100$ *and* $\beta J_0 = 8.0$. *Note that the external field h is lower so that it induces faster phase transitions.*

ogy that enables deriving higher-order schemes when required. Next we proceed to explore the connections and implications of these methodologies to coarse-graining of macromolecular systems. Coarse-graining of macromolecular systems has attracted considerable attention in polymer science and engineering [17, 20]. Key challenges include the presence of complex short- and long-range interactions similar to (3.6), as well as the off-lattice nature of the models. In this section we discuss the connection and extension of the analytical and computational strategies for coarse-graining lattice systems presented in this paper as well as in [9, 14, 12] to more complex off-lattice macromolecular systems, specifically coarse-graining of polymer systems.

6.1. McCoy–Curro scheme for off-lattice systems. We present a coarse-graining procedure for the united atom (UA) model, which is known in the polymer science coarse-graining literature as the McCoy–Curro scheme [2, 4, 6, 23]. This scheme was first developed for the coarse-graining of small molecules in [19] and later extended to polymers in [4]. The interactions in the system consist of bonded interactions (H_b), which are *short-range* interactions between neighboring atoms in an individual polymer chain. They are defined by the potential U_b, which is a function of the bond length r, the bond angle Θ, and the torsion angle Φ, i.e., $H_b = \sum U_b(r, \Theta, \Phi)$. Another contribution to the Hamiltonian is from nonbonded interactions (H_{nb}), which represent *long-range* interactions between atoms of different chains and are typically modeled with a Lennard-Jones two-body potential U_{nb}. The Hamiltonian also includes total kinetic energy (H_{kin}) of the system, Coulomb interactions (H_{coul}) associated with charged macromolecules, and terms which describe the interactions associated

with walls (H_{wall}). The entire UA model consists of n macromolecules in a fixed volume at the inverse temperature β, and each macromolecule consists of m atoms. Hence the system consists of $N = nm$ microscopic particles at positions denoted by $X = (x_1, \dots, x_N)$, where $x_i \in \mathbb{R}^3$ is the position of the ith atom. The Hamiltonian of the system is given by

$$H_N(X) = H_b(X) + H_{nb}(X) + H_{coul}(X) + H_{wall}(X) + H_{kin}(X)\,. \tag{6.1}$$

The corresponding canonical Gibbs measure is given by

$$\mu(dX) = \frac{1}{Z} e^{-\beta H_N(X)} \prod_i dx_i\,, \quad Z = \int e^{-\beta H_N(X)} \prod_i dx_i\,. \tag{6.2}$$

The coarse-graining of this system is carried out by grouping l of the UAs together by creating chains consisting of a total of $M = N/l$ "superatoms." The positions of the CG particles are denoted by the coarse variables $Q = (q_1, \dots, q_M)$, where $q_i \in \mathbb{R}^3$ is the position of the center of mass of the ith superatom. Similarly to the lattice case the first task consists in deriving the coarse-grained Hamiltonian and the corresponding coarse-grained interaction potentials. The exactly coarse-grained Hamiltonian $\bar{H}_M(Q)$ is defined as in the lattice case (see (1.4)):

$$e^{-\beta \bar{H}_M(Q)} = \int_{\{X \in \mathbf{X} | \mathbf{F}X = Q\}} e^{-\beta H_N(X)}\, dX\,, \tag{6.3}$$

where $\mathbf{F}$ denotes the projection of the microscopic variable to the coarse variable.

For the sake of simplicity we focus on the case where only bonded and nonbonded interactions are present in the Hamiltonian, i.e., $H_N(X) = H_b(X) + H_{nb}(X)$. From the expression (6.3) we have

$$\bar{H}_M(Q) = -\frac{1}{\beta} \log \int_{\{X \in \mathbf{X} | \mathbf{F}X = Q\}} e^{-\beta(H_b(X) + H_{nb}(X))}\, dX\,. \tag{6.4}$$

Although (6.4) is not additive, the following approximation is made:

$$\bar{H}_M(X) = \bar{H}_b(X) + \bar{H}_{nb}(X)\,, \tag{6.5}$$

where $\bar{H}_b$, $\bar{H}_{nb}$ are the coarse-grained bonded and nonbonded Hamiltonians H_b and H_{nb}, respectively, both to be calculated in the following step. Since β is proportional to the inverse temperature, the approximation for (6.4) is expected to hold only at higher temperatures. In the second step, we assume $\bar{H}_b = \sum \bar{U}_b$ and $\bar{H}_{nb} = \sum \bar{U}_{nb}$, respectively, where $\bar{U}_b$ and $\bar{U}_{nb}$ are the corresponding coarse-grained potentials. It is assumed that $\bar{U}_b(r, \Theta, \Phi)$ can be further simplified and can be written as $\bar{U}_b(r, \Theta, \Phi) = \bar{U}_b^r + \bar{U}_b^\Theta + \bar{U}_b^\Phi$. Similarly, it is assumed that the long-range term $\bar{U}_{nb}$ depends only on binary interactions between coarse-grained particles and is given by the average of the interactions between two isolated molecules at positions q_i, q_j,

$$\bar{U}_{nb}(|q_i - q_j|) = -\frac{1}{\beta} \log \int_{\{X : \mathbf{F}X = (q_i, q_j)\}} e^{-\beta \tilde{H}_{nb}}\, dX\,, \tag{6.6}$$

where the Hamiltonian $\tilde{H}_{nb}$ is the detailed description of two isolated molecules. In other words, $\bar{U}_{nb}(|q_i - q_j|)$ is a two-body coarse-grained interaction.

These simplifying assumptions allow for the breakup of the intractable computational evaluation of (6.4). For instance, (6.6) is calculated through atomistic simulations, performed on only *two* isolated oligomers by sampling the phase space. Thus we can obtain the PDF between the coarse-grained particles at a given distance, and the effective bonded coarse-grained potential $\bar{U}_{nb}$ is subsequently calculated by taking a logarithm, similarly to (6.4). All of these calculations need to be repeated whenever the parameters N, V, and T are changed.

On the other hand, from a numerical analysis perspective, the aforementioned assumptions are nothing but numerical approximations of (6.4). When compared to direct numerical simulations, this coarse-graining approach yields good results in some regimes; however, deviations can also be observed both in the structure and dynamics [1, 6]. Differences could be attributed to the simplifying set of assumptions that are necessary for the derivation of coarse-grained potentials such as (6.6). For example, as discussed earlier in this section, this error is expected to be small in relatively higher temperatures, when the approximation (6.5) is justified, but this is not necessarily true at lower temperatures. A detailed understanding of the parameter regimes where the approximations are valid is still lacking for the macromolecular case. Nonetheless, our error analysis for lattice systems directly addresses this issue in terms of Schemes 2.1 and 2.2. Next we discuss the connection of such schemes to the McCoy–Curro methodology.

6.2. McCoy–Curro scheme on the lattice. In order to better understand the McCoy–Curro scheme, we present it in the context of lattice systems, drawing some analogies between the coarse-graining of polymer chains and coarse-graining in lattice systems. An important fact that is highlighted in section 3 is the role of the multibody interactions when studying complex interactions which are absent in the present coarse-graining methods applied to macromolecular systems (see (6.6)). According to the McCoy–Curro scheme the coarse-grained Hamiltonian is given by

$$\bar{H}^{MCC}(\eta) = -\sum_{k,\, l\in\bar{\Lambda}_M} \bar{U}^{MCC}(\eta_k, \eta_l, |k-l|)\,, \tag{6.7}$$

and, in analogy to (6.6),

$$\bar{U}^{MCC}(\eta_k, \eta_l, |k-l|) = -\frac{1}{\beta}\log\left(\mathbb{E}\left[e^{-\beta H_{C_k,C_l}(\sigma)}|\eta_k,\, \eta_l\right]\right)\,, \tag{6.8}$$

where the Hamiltonian between two isolated coarse cells is defined as

$$H_{C_k,C_l}(\sigma) = -\frac{1}{2}\sum_{x\in C_k,\, y\in C_l} J(x-y)\sigma(x)\sigma(y)\,. \tag{6.9}$$

If we rewrite the $U^{MCC}(\eta_k, \eta_l, |k-l|)$ defined in (6.8) in terms $\bar{J}(k,l)$, then we obtain

$$\begin{aligned}\bar{U}^{MCC}(\eta_k, \eta_l, |k-l|) &= \frac{1}{2}\bar{J}(k,l)\,\eta_k\,\eta_l - \frac{1}{\beta}\log(\mathbb{E}[e^{-\beta\Delta J_{kl}(\sigma)}|\eta_k,\, \eta_l]) \\ &= \frac{1}{2}\bar{J}(k,l)\,\eta_k\,\eta_l - \frac{1}{\beta}\log\left(\int_{\{\sigma:\mathbf{F}(\sigma)=(\eta_k,\eta_l)\}} e^{-\beta\Delta J_{kl}(\sigma)}P(d\sigma|\eta_k,\, \eta_l)\right).\end{aligned} \tag{6.10}$$

Equation (6.10) is similar to (2.6); however, it is not defined on the entire lattice. Expanding as in section 2.3, we obtain

$$\begin{aligned}\bar{H}^{MCC}(\eta) &= -\sum_{k,\,l\in\bar{\Lambda}_M}\frac{1}{2}\bar{J}(k,l)\,\eta_k\,\eta_l+\sum_{k,l}\frac{1}{\beta}\log(\mathbb{E}[e^{-\beta\Delta J_{kl}(\sigma)}\ \ |\eta_k,\,\eta_l)])\\ &= -\sum_{k,\,l\in\bar{\Lambda}_M}\frac{1}{2}\bar{J}(k,l)\,\eta_k\,\eta_l+\sum_{k,l}\frac{1}{\beta}\log[1+\mathbb{E}[(-\beta\Delta J_{kl}(\sigma))^2]+\cdots]\\ &= -\sum_{k,\,l\in\bar{\Lambda}_M}\frac{1}{2}\bar{J}(k,l)\,\eta_k\,\eta_l+\sum_{k,l}\frac{\beta}{2}\mathbb{E}[(\Delta J_{kl}(\sigma))^2]+\cdots\\ &= \bar{H}_M^{(0)}(\eta)+\bar{H}_M^{(1)}(\eta)+\cdots(\text{ higher-order two-body interactions}).\end{aligned}\tag{6.11}$$

From the calculations above it follows that the McCoy–Curro scheme is asymptotically identical to a scheme using $\bar{H}_M^0(\eta)$ and $\bar{H}_M^1(\eta)$ given in section 2.4. However, the three-body terms given by $\bar{H}_M^2(\eta)$ in Scheme 2.2 are absent. As we have seen in sections 3 and 5, including the three-body interactions is crucial to obtain higher accuracy, especially in low temperature regimes.

It should also be noted that from the computational point of view the schemes in section 2.4 are much more efficient than the McCoy–Curro scheme. Implementing the McCoy–Curro scheme requires calculating $\bar{U}^{CG}(\eta_k,\eta_l,|k-l|)$, using (6.8) over all possible ranges of $\eta_k,\eta_l,|k-l|$, and repeating all of the calculations for each temperature β.

In Figure 9 we present the results for the simulations ignoring the three-body terms, i.e., using only $\bar{H}_M^0(\eta)$ and $\bar{H}_M^1(\eta)$. The setup of the simulation is the same as in section 5.2. It is observed that using only $\bar{H}_M^0(\eta)$ and $\bar{H}_M^1(\eta)$ the scheme fails to capture both antiferromagnetic behavior and the double hysteresis exhibited by the microscopic process. This observation further emphasizes the importance of multibody interactions for deriving higher-order coarse-graining schemes.

7. Conclusion. A main premise of this paper as well as its precursor [14] is to view coarse-graining as a numerical approximation of coarse observables, which otherwise would have to be calculated exactly, using computationally intractable microscopic simulations. As expected, these approximations should produce numerical error that needs to be assessed and controlled. In [14] we derived such coarse-graining schemes as truncations of cluster expansions of the renormalization map around an initial coarse-graining approximation, e.g., (1.5) in the context of this paper. The higher-order terms in these expansions contain multibody interactions, given in terms of explicit formulae, e.g., Scheme 2.2. Coarse-graining schemes in the applied sciences literature include only two-body terms between coarse variables, as multibody terms are hard to evaluate computationally, even if an analytical formula is known, as in [14]. On the other hand, it is also understood that such terms can be crucial especially at lower temperatures.

Here we study these two related issues. We focus our attention on lattice systems as a paradigm for coarse-graining of an extended stochastic system; however, our general approach is expected to be applicable to other examples of coarse-graining such as in macromolecular systems. First, we study the relative importance of multibody versus two-body coarse-grained interactions and their dependence on the details of the particle-particle interaction potential, the temperature, and other parameters. Second, we derive strategies for the efficient implementation of multibody interactions

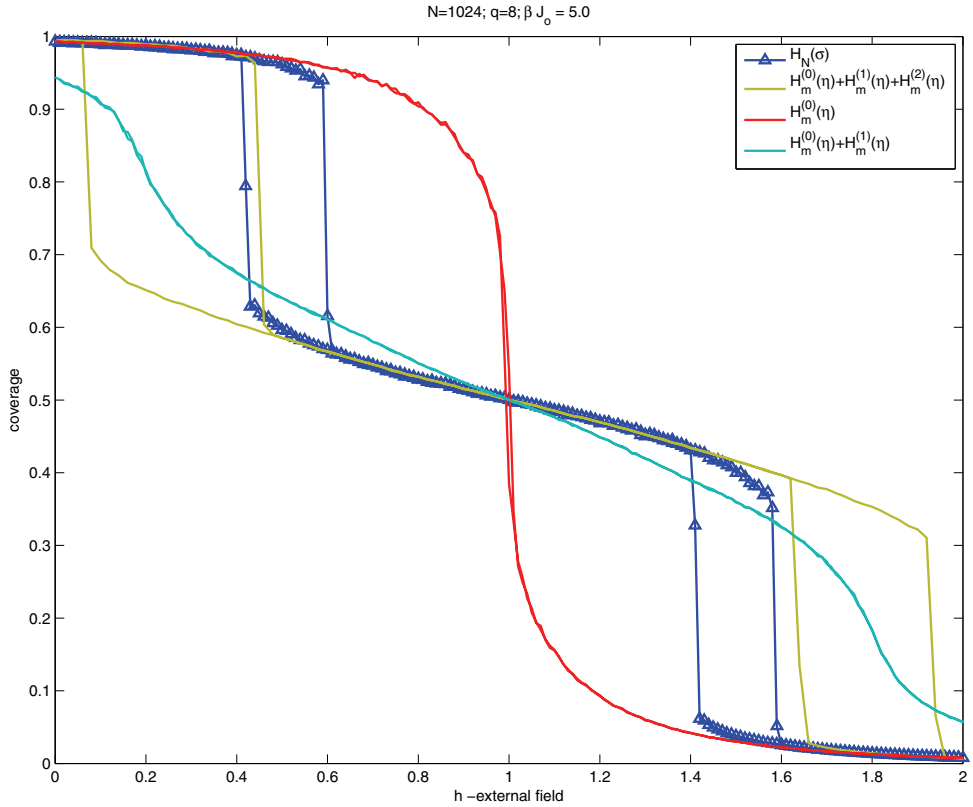

FIG. 9. *Comparison of the hysteresis behavior using a Lennard–Jones-type potential of the microscopic process (MC), coarse-grained process using Scheme* 2.2 $\left(\bar{H}^0_M(\eta)+\bar{H}^1_M(\eta)+\bar{H}^2_M(\eta)\right)$*, the coarse-grained process Scheme* 2.1 $\left(\bar{H}^0_M(\eta)\right)$*, and the coarse-grained process using only* $\bar{H}^0_M(\eta)$ *and* $\bar{H}^1_M(\eta)$ *for* $\beta J_0 = 5.0$*. We note that with corrections using only* $\bar{H}^0_M(\eta)$ *and* $\bar{H}^1_M(\eta)$ *the simulation fails to capture the antiferromagnetic behavior and double hysteresis exhibited by the microscopic process.*

based on our error analysis, by either (a) compressing the multibody interactions by truncating them within arbitrary tolerance, or (b) decomposing general interacting potentials into a short-range and singular part, as well as a long-range, smooth part; multibody terms are necessary only for the former term, but they are computationally inexpensive due to the short-range interactions.

An alternative perspective based on the above decompositions is presented in the forthcoming [13], designed specifically for systems with combined short- and long-range interactions such as (5.2). As we observed in the comparison of Figures 4 and 5, even the multibody Scheme 2.2 may be insufficient to predict quantitatively, at low temperatures, the exact hysteresis diagram. The principal idea in [13] is to build a better initial guess than (1.5) for the cluster expansion (1.7). For this purpose we introduce a different prior P_N which already includes *multibody* coarse cell correlations, associated with the short-range interactions.

REFERENCES

[1] C. F. ABRAMS AND K. KREMER, *The effect of bond length on the structure of dense bead–spring*

polymer melts, J. Chem. Phys., 115 (2001), pp. 2776–2785.
[2] R. L. C. Akkermans and W. J. Briels, *Coarse-grained interactions in polymer melts: A variational approach*, J. Chem. Phys., 115 (2001), pp. 6210–6219.
[3] A. Chatterjee and D. Vlachos, *An overview of spatial microscopic and accelerated kinetic Monte Carlo methods*, J. Comput. Aided Mater. Des., 14 (2007), pp. 253–308.
[4] H. Fukunaga, J.-ichi Takimoto, and M. Doi, *A coarse-graining procedure for flexible polymer chains with bonded and nonbonded interactions*, J. Chem. Phys., 116 (2002), pp. 8183–8190.
[5] N. Goldenfeld, *Lectures on Phase Transitions and the Renormalization Group*, Vol. 85, Addison–Wesley, New York, 1992.
[6] V. A. Harmandaris, N. P. Adhikari, N. F. A. van der Vegt, and K. Kremer, *Hierarchical modeling of polysterene: From atomistic to coarse-grained simulations*, Macromolecules, 39 (2006), pp. 6708–6719.
[7] L. Kadanoff, *Scaling laws for Ising models near* t_c, Physics, 2 (1966), pp. 263–272.
[8] M. Kardar, *Crossover to equivalent-neighbor multicritical behavior in arbitrary dimensions*, Phys. Rev. B, 28 (1983), pp. 244–246.
[9] M. A. Katsoulakis, A. J. Majda, and D. G. Vlachos, *Coarse-grained stochastic processes and Monte Carlo simulations in lattice systems*, J. Comput. Phys., 112 (2003), pp. 250–278.
[10] M. A. Katsoulakis, A. J. Majda, and D. G. Vlachos, *Coarse-grained stochastic processes for microscopic lattice systems*, Proc. Natl. Acad. Sci. USA, 100 (2003), pp. 782–787.
[11] M. A. Katsoulakis, P. Plecháč, and A. Sopasakis, *Error analysis of coarse-graining for stochastic lattice dynamics*, SIAM J. Numer. Anal., 44 (2006), pp. 2270–2296.
[12] M. A. Katsoulakis, P. Plecháč, L. Rey-Bellet, and D. K. Tsagkarogiannis, *Mathematical strategies in the coarse-graining of extensive systems: Error quantification and adaptivity*, J. Non-Newtonian Fluid Mech., 152 (2008), pp. 101–112.
[13] M. A. Katsoulakis, L. Rey-Bellet, P. Plecháč, and D. K. Tsagkarogiannis, *Coarse-Graining Schemes for Stochastic Lattice Systems with Short and Long Range Interactions*, preprint.
[14] M. A. Katsoulakis, L. Rey-Bellet, P. Plecháč, and D. Tsagkarogiannis, *Coarse-graining schemes and a posteriori error estimates for stochastic lattice systems*, M2AN Math. Model. Numer. Anal., 41 (2006), pp. 627–660.
[15] M. A. Katsoulakis and A. Szepessy, *Stochastic hydrodynamic limits of particle systems*, Commun. Math. Sci., 4 (2006), pp. 513–549.
[16] M. A. Katsoulakis and J. Trashorras, *Information loss in coarse-graining of stochastic particle dynamics*, J. Stat. Phys., 122 (2006), pp. 115–135.
[17] K. Kremer and F. Müller-Plathe, *Multiscale problems in polymer science: Simulation approaches*, MRS Bull., 26 (2001), pp. 205–210.
[18] D. P. Landau and K. Binder, *A Guide to Monte Carlo Simulations in Statistical Physics*, Cambridge University Press, Cambridge, UK, 2000.
[19] J. McCoy and J. Curro, *Mapping of explicit atom onto united atom potentials*, Macromolecules, 31 (1998), pp. 9362–9368.
[20] F. Müller-Plathe, *Coarse-graining in polymer simulation: From the atomistic to the mesoscale and back*, Chem. Phys. Chem., 3 (2002), pp. 754–769.
[21] I. Pivkin and G. Karniadakis, *Coarse-graining limits in open and wall-bounded dissipative particle dynamics systems*, J. Chem. Phys., 124 (2006), 184101.
[22] B. Simon, *The Statistical Mechanics of Lattice Gases. Vol.* I, Princeton Ser. Phys., Princeton University Press, Princeton, NJ, 1993.
[23] W. Tschöp, K. Kremer, O. Hahn, J. Batoulis, and T. Bürger, *Simulation of polymer melts.* I. *Coarse-graining procedure for polycarbonates*, Acta Polym., 49 (1998), pp. 61–74.
[24] B. Turkington, *Statistical equilibrium measures and coherent states in two-dimensional turbulence*, Comm. Pure Appl. Math., 52 (1999), pp. 781–809.